REPORT DOCUMENTATION PAGE

Form Approved OMB No. 0704-0188

1. REPORT DATE *(DD-MM-YYYY)*	2. REPORT TYPE	3. DATES COVERED *(From – To)*
03-09-2003	Final Report	18 August 2002 - 18-Aug-03

4. TITLE AND SUBTITLE

Transverse resistivity of YBCO coated conductors for AC use

5a. CONTRACT NUMBER
FA8655-02-M4065

5b. GRANT NUMBER

5c. PROGRAM ELEMENT NUMBER

6. AUTHOR(S)

Dr. Milan Polak

5d. PROJECT NUMBER

5d. TASK NUMBER

5e. WORK UNIT NUMBER

7. PERFORMING ORGANIZATION NAME(S) AND ADDRESS(ES)

Institute of Electrical Engineering
Dubravska 9
Bratislava 84104
Slovak Republic

8. PERFORMING ORGANIZATION REPORT NUMBER

N/A

9. SPONSORING/MONITORING AGENCY NAME(S) AND ADDRESS(ES)

EOARD
PSC 802 BOX 14
FPO 09499-0014

10. SPONSOR/MONITOR'S ACRONYM(S)

11. SPONSOR/MONITOR'S REPORT NUMBER(S)
SPC 02-4065

12. DISTRIBUTION/AVAILABILITY STATEMENT

Approved for public release; distribution is unlimited.

13. SUPPLEMENTARY NOTES

14. ABSTRACT

This report results from a contract tasking Institute of Electrical Engineering as follows: The contractor will investigate transverse resistivity and factors controlling it in Yttrium Barium Copper Oxide (YBCO) based alternating current (AC) superconductors. This investigation will study the properties of metallic layers deposited on YBCO and the boundary resistivity of the boundary YBCO/metal. The results of this investigation will assist in determining the optimal amount and location of the stabilizing metal assuring a sufficient stability and acceptable AC losses. Effect of local inhomogeneities on the behavior of the conductors will be also studied.

15. SUBJECT TERMS
EOARD, Aircraft Subsystem, Power, Superconductivity

16. SECURITY CLASSIFICATION OF:			17. LIMITATION OF ABSTRACT	18, NUMBER OF PAGES	19a. NAME OF RESPONSIBLE PERSON
a. REPORT	b. ABSTRACT	c. THIS PAGE			MICHAEL KJ MILLIGAN, Lt Col, USAF
UNCLAS	UNCLAS	UNCLAS	UL	30	19b. TELEPHONE NUMBER *(Include area code)* +44 (0)20 7514 4955

Institute of Electrical Engineering, Department of Electrodynamics of Superconductors, Slovak Academy of Sciences, Bratislava, Slovakia

TRANSVERSE RESISTIVITY OF YBCO COATED CONDUCTORS FOR AC USE

Final Report

This report includes the results obtained in the frame of the contract with European Office of Aerospace Research and Development (EOARD).
Contract order number: F61775-02-W4065, SPC 02-4065

Content:

Bratislava, August 2003

1. Objectives of the work

The objectives of the contract defined in the technical proposal are the following:

- To investigate the effect of patterning on the properties of filaments exposed to DC external magnetic field
- To investigate the effect of patterning on the properties of the striated conductor exposed to AC external magnetic field with frequencies of the order of 100 Hz
- To prepare and study transverse resistivity in with samples with different architecture (continuous metal layer, metal layer deposited on the surface of filament only)
- Determination of the resistivity of YBCO/normal metal layer by measuring the current transfer length and resistance of the metal layer
- Development of measurement set up for AC loss measurements

The results obtained in the frame of this contract:

2. Samples

According to the project program a part of samples should be prepared by the Air Force Laboratories in Dayton, Ohio. We received and studied 2 samples: 1 YBCO tape on LaAlO substrate and 1 Ag/YBCO/Ni sample. In the actual period we received also samples from the University of Wuppertal, group of Dr. Burckhardt Moenter (Mrs. D. Wehler). The samples were prepared according to the following ideas:

- Filamentary YBCO/LaAlO samples not covered by metal layer. With these samples we studied the dependence of hysteresis losses on frequency. Any coupling losses are present.
- Filamentary YBCO/LaAlO samples covered by a continuous layer of normal metal (Ag, Au).These samples serve to the study of coupling loss behavior, measurement of transverse resistivity as well as to the study of the influence of sample annealing in O_2 on both parameters.
- Samples of the substrate (Ni, NiW) determined to studies of magnetization losses in the substrates
- Samples of filamentary YBCO/Ni not covered by normal metal for studies of hysteresis losses consisting of YBCO losses and substrate losses. YBCO and substrate interact.
- Samples of filamentary YBCO/Ni covered by a normal metal layer. Total losses in external magnetic field will be measured.

More details about the prepared samples are given in the following tables:

Samples YBCO on LaAlO (box 1)

sample number	filament number	dimensions (μm)	metal covering metal/thickness	sample width/length	Note

		filament/gap		(mm)	
R-LaAlO-1a	60	~50/15	free surface + telon	3.4 x 40	broken, 3 pieces glued on G10 plate
R-LaAlO-1b	60	~50/15	Ag	4.4 x 40	
R-LaAlO-1c	60	~50/15	free surface	3.4 x 40	
R-LaAlO-1d	7	500/20	Au-filaments only	4 x 40	substrate dimensions !!
R-LaAlO-1e	1	1500	free surface	~ 2 x 40	
R-LaAlO-1f	1	1600	Au	~2 x 40	for boundary resistivity experiments
sapphire/ YBCO/Ag	1	1770	Ag	~2 x 40	for boundary resistivity experiments

RABiTS YBCO filamentary samples (box 2)

sample number	filament number	dimensions (μm) filament/gap	metal covering metal/thickness	sample width/length (mm)	Note
NiCYC 66	7	500/20	free surface	3.6/40	
NiCYC 65	30	100/ 20	free surface		wider filaments at the edges (2x)
NiCYC 67	60	50/10	free surface	3.4 x 40	some areas not well etched, continuous layer
NiCYC 64A			free surface		not etched, some etching signs visible
NiCYC 64B		structure not visible	Ag		glued to G10 plate

RABiTS YBCO concentric rings, mean ring diameter 3 mm (box 2)

sample number	filament number	filament width/gap (μm)	surface		Note
NiCYC 68/1	1	500	free		

NiCYC 68/2	5	80/20	free		
NiCYC 68/3	10	40/10	free		
B272-1	1	10 mm	free		not structured, as prepared

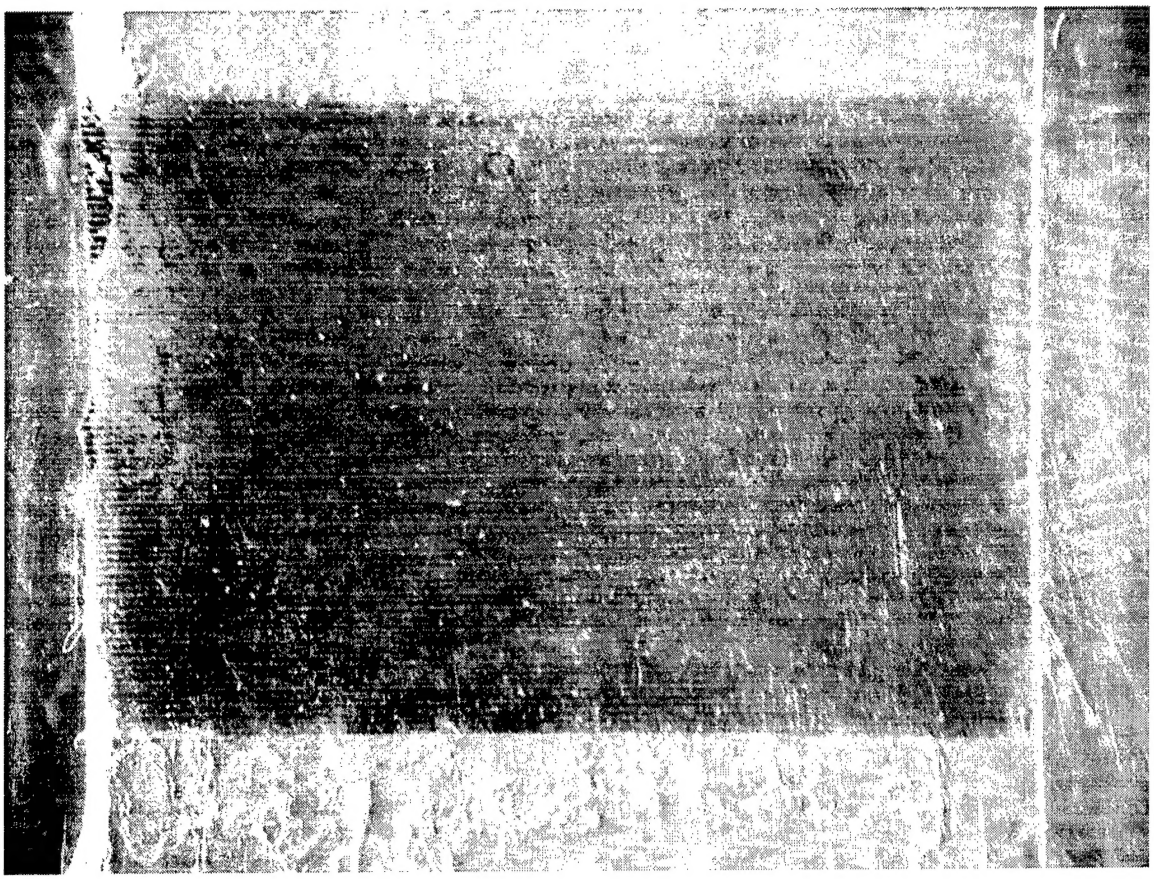

Microphotograph of sample W82L3 covered by Ay layer

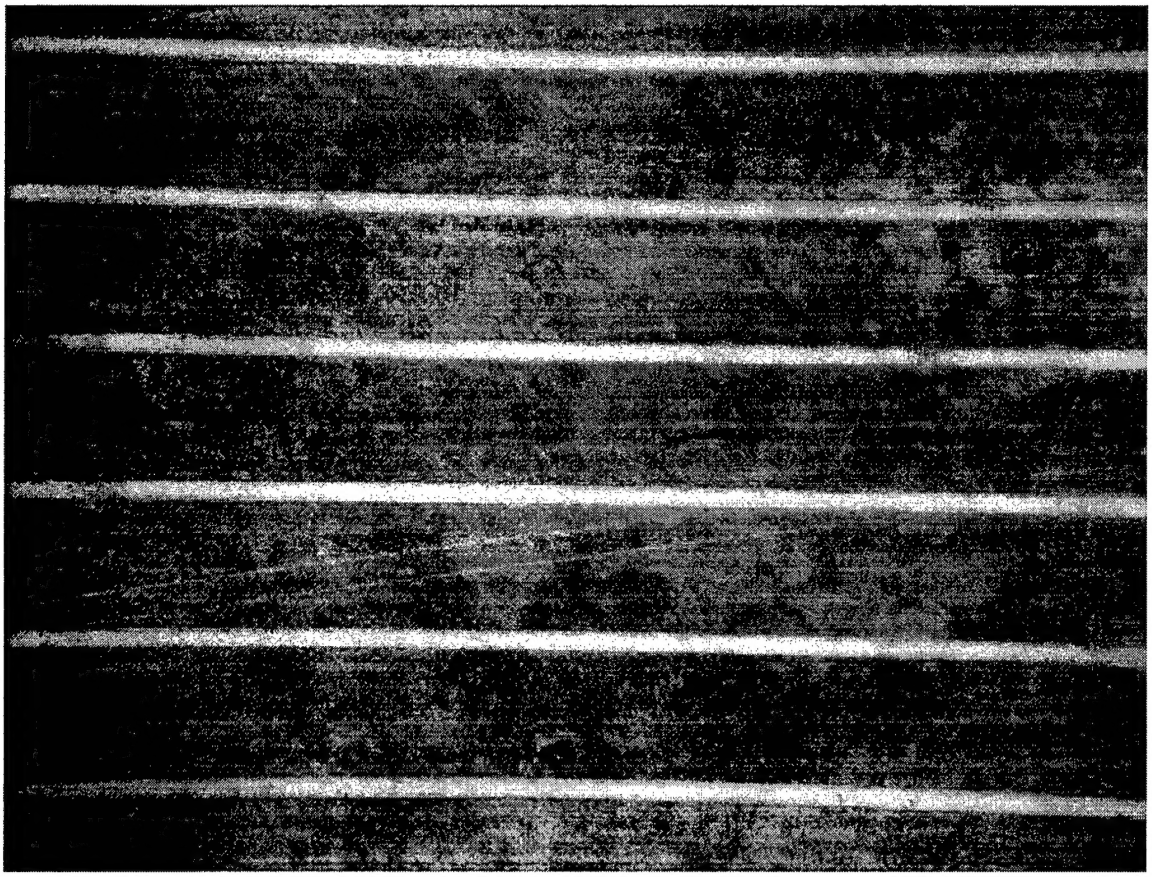

Detail of filamentary structure of sample W 82L3

3. Measuring methods and set-up

3.1. Measurement of critical current density in circular narrow filaments

We have designed and tested a method using samples in the form of concentric rings with small filament width. External magnetic field induces currents in the rings, which produce magnetic field. This field is measured by a small active area Hall probe.
The main advantage of the method is that it does not need contacts which could damage the fine filaments and modify the filament properties.

3.2. Measurement of magnetic field profile in the vicinity of striated samples, determination of J_c

The magnetization currents are induced in the filaments by the change of the external magnetic field. Each filament produces its own field. The component of this field perpendicular to the plane of the tape is measured by micro Hall Probe. We used a numerical method to determine J_c in the filaments.

3.3. Determination of the boundary resistivity YBCO/metal from the current transfer length

We used the same method as that used for Bi-2223/Ag [M. Polak, W. Zhang, J. Parrell, X. Y. Cai, A. Polyanskii, E. E. Hellstrom, D. C. Larbalestier, M. Majoros, Current transfer length and the origin of linear components in the voltage - current curves of Ag-sheathed BSCCO composites, Supercond. Sci. Technol. 10 (1997) 769-777]. It is based on the measurement of the potential profile in the vicinity of the current contact by means of several potential taps located in different distances from the current contact, x.

The current transfer length, Λ, is given by

$$\Lambda = (R_{b1}/R_{Ag1})^{1/2} \qquad (1)$$

where R_{b1} is the current transfer resistance per unit tape length and R_{Ag1} is the resistance of the metal layer per unit length. The value of Λ is determined from the potential profile measured at a current I. Knowing Λ and R_{Ag1} we can obtain R_{b1} from Eq.(1).
The effective resistivity of the metal/YBCO boundary, r_b, can be determined from

$$r_b = R_{b1}\, A_{b1} \qquad (2)$$

where A_{b1} is the area of the boundary per unit length.

3.4. Direct measurement of the transverse resistivity

We study transverse resistivity of YBCO filamentary tapes covered by continuous Au or Ag films by two different ways:

a. the filamentary structure is covered by a continuous metallic film
b. each filament is covered by the metallic layer, the layers are not interconnected

Two types of YBCO filamentary tapes were used:

- YBCO on $LaAlO_3$ substrates
- YBCO/buffer layers/Ni
-

In the case of continuous Ag layer covering filaments the total resistance between 2 points across the filamentary tape can be determined as:

$R_{12} = (R_f + R_g)\, N_f$

whereR_f is he resistance of the section conting the filament shunted bAg layer which are joied via the boundary layer with resistivity ρ_b, R_f is the resistance of Ag layer between two filaments, N_f is the number of filaments between points 1 and 2.

The resistance R_f is strongly affected by ρ_b. Due to finite value of it only a part of the current I flows into the filament and back.

The resistance R_{Ag} is

$R_{Ag} = N_f\, \rho_{Ag}\, [2g/(t_{Ag}\, w)]$

where ρ_{Ag} and t_{Ag} is the resistivity and thickness of Ag layer, w is the sample width, 2g is the gap width.

We have designed and built special sample holder in which the sample of the model conductor is placed. The current in the sample flows perpendicular to the filaments. The current path simulates that followed by coupling currents. The sample holder can be also placed in an external magnetic field.

3.5. Measurement of AC losses in external magnetic fields

Frequency dependence of total losses allows us to determine the time constant of coupling currents and the transverse resistivity, ρ_{tr}. We have built and tested experimental set up for four measurement methods:

- method using pick-up coils and analog integration (L-1)
- method using pick-up coils and lock-in nanovoltmeter or a selective nanovoltmeter to determine the first harmonic of the voltage signal
- method using Hall probes to measure magnetization via magnetic field measurement
- method suing the Fourier analysis of the voltage signal to determine the first harmonic proportional to losses.

We will compare the results, advantages and disadvantages of these methods and use the most suitable one for standard experiments on samples of AC YBCO conductors.
The tests realized up to now showed that the main problem of the loss measurements will be the sensitivity of the method.

The basic element of all systems is the copper magnet producing the external magnetic field with variable frequency. We have built two magnets with the inner diameter of 60 mm and different inductance. To achieve fields of the order of 0.1 T at 77 K and frequencies up to 400 Hz it is necessary to use capacitors C in series with the coil. By a suitable choice of C the coil and capacitor operate in the resonance mode and the total voltage of this L,C circuit allows to achieve high currents at low voltage of the power supply.

4. Results

4.1. Critical current density in narrow filaments

Low loss YBCO based flexible conductors for AC operation must have a filamentary structure. MO images of structured YBCO films showed that the flux penetration is less homogeneous in YBCO filaments on Ni substrates than that in filaments on LaAlO, which indicates that the patterning may affect the critical current density in narrow filaments. To see the effect of patterning we studied a possible effect of filament width on the critical current per unit filament width (I_{c1}) and hysteresis losses (P_h) in YBCO rings with various widths ranging from 0.3 mm down to 0.02 mm.

Samples were prepared from YBCO layers deposited on $LaAlO_3$ and also on Ni substrates. The first set of samples was prepared from a 0.328 μm thick YBCO layer deposited on $LaAlO_3$ substrates with dimensions of 1 x 2 cm. Sample R was a reference sample with dimensions of 5.3 x 14 mm. Using optical litography and wet etching we prepared rings with the mean diameter of 3 mm and width 300 μm (sample 1), 51 μm (sample 2) and 20 μm (sample 3). Rings with 3 mm were prepared also from 0.6 μm thick YBCO layers deposited on 0.1 mm thick Ni substrates via a buffer layer: ring with 300 μm (sample 4) and 100 μm (sample 5).
To avoid problems with current contacts, the current in the rings was induced by external magnetic field and electric field-current characteristics were determined by a Hall probe method.

We measured hysteresis loops $B_z(B_e)$ with triangular waves of the external magnetic field $0 \rightarrow 75$ mT$\rightarrow 0 \rightarrow$(-75 mT) $\rightarrow 0$ (dB_e/dt =const) with 5 different frequencies (100 mHz, 20 mHz, 5 mHz, 2 mHz and 1 mHz).
From the hysteresis loops of rings 1, 2 and 3 we determined E-I curves at B_e=0. These curves are shown in Fig. 4.1.1 The straight lines are $E \sim I_1^n$ curves with n=18. The ratio between the highest (sample 2) and lowest value of J_c is ~1.9. We believe that the different J_c values are mainly due to an inhomogeneous distribution of the critical current density in the original layer. This explanation is also supported by the fact that the largest sample R has the lowest J_c.

We also measured the distribution of the remanent field B_z in the radial direction at various distances z. The critical current densities were deduced from $B_z(r=0)$. The results for ring 1 are shown in Fig. 4.1.2 and similar families of curves were obtained for other samples.
It is also interesting to note that the magnetization currents induced in sample R at 20 Hz are higher by a factor 1.36 than those induced at 0.1 Hz. The hysteresis losses must be also determined at the operating frequency of the AC conductor to avoid a greatly underestimating them.

We believe that the variation of critical current density in filaments prepared from YBCO layers deposited on $LaAlO_3$ substrates can be ascribed to the inhomogeneity of the origin layer. No

substantial reduction of the critical current density in the 20 microns wide filament was observed.
Hysteresis losses in filaments of YBCO on $LaAlO_3$ decreased with decreasing filament width and increased with increasing frequency. In the narrowest filament they were
$\sim 10^{-7}$ J/m, cycle at 100 mHz and field amplitude of 75 mT.
For YBCO rings on Ni substrates we were able to measure the critical currents of the sample 300 microns wide only, as the signal from the substrate considerably affected the magnetic field in the vicinity of the narrower samples. To reduce the effect of Ni in experiments with YBCO on Ni, ring samples with smaller filament width should have the form of several concentric rings.

The results were presented at Applied Superconductivity Conference 2002 and published:

M. Polak, L. Krempasky, E. Demencik, D. Wehler, S. Kreiskott, B. Moenter, A. Polyanskii and D.C. Larbalestier, IEEE Trans. on Appl. Superc. 13 (2003) 2595

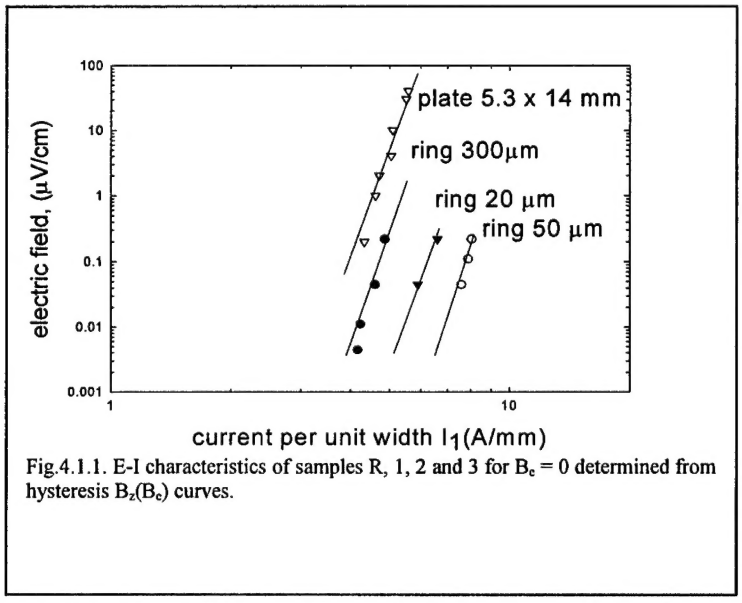

Fig.4.1.1. E-I characteristics of samples R, 1, 2 and 3 for $B_e = 0$ determined from hysteresis $B_z(B_e)$ curves.

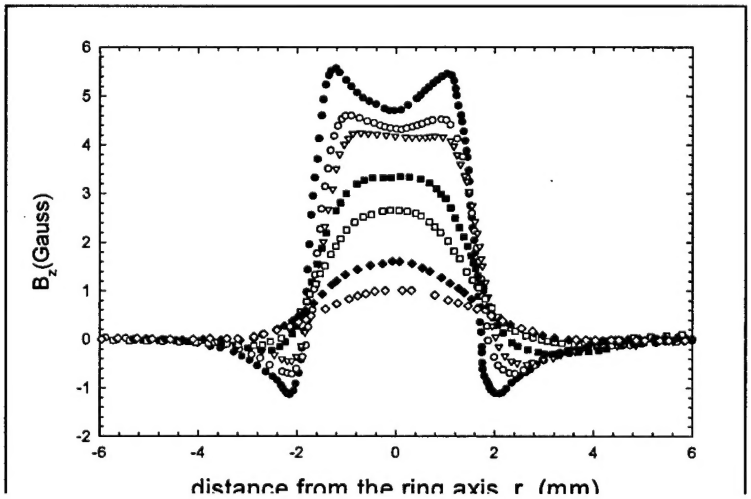

4.2.Magnetic measurements with striated samples

4.3. Boundary resistivity in samples covered by Au and Ag

We tested the effect of the sample annealing in O_2 on the boundary resistivity. The results are shown in the following Figure 4.3.1. Annealed samples show shorter current transfer length and, consequently, smaller boundary resistivity.

Voltage V_{n-r} between point "n" and a reference point, "r", vs distance "x" of "n" from the sample end (current contact). The current I=0.5 A.

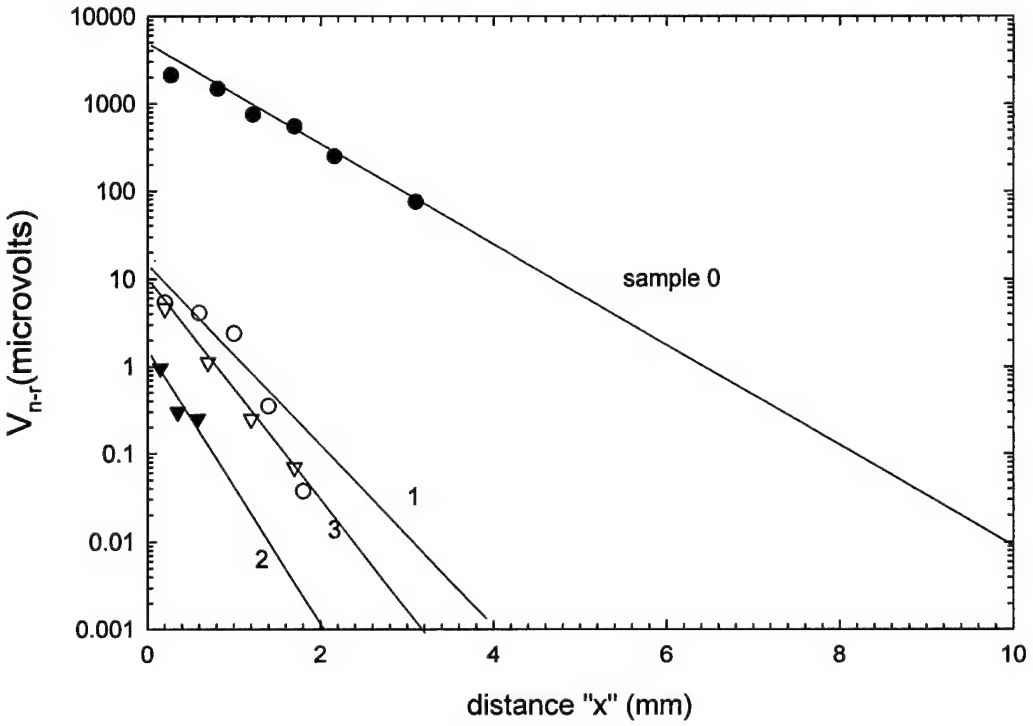

- YBCO 0 - reference sample:YBCO/Au on LaAlO, not annealed
- YBCO 1- sample annealed 300^0 C for 20 min
- YBCO 2 - sample annealed 350^{0}C for 20 min
- YBCO 3 - sample annealed at 400^{0}C for 20 min

Fig. 4.3.1

4.4. Transverse resistivity measured in samples "as received" and heat treated samples

YBCO filamentary tapes can be covered by Au or Ag films by two different ways:

- the filamentary structure is covered by a continuous metallic film (see Fig.4.4.1)
- each filament is covered by the metallic layer, the layers are not interconnected (see Fig.4.4.2)

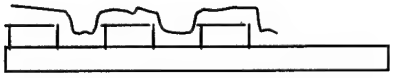

Fig. 4.4.1

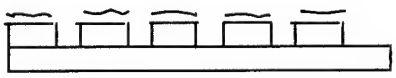

Fig.4.4.2

Two types of YBCO filamentary tapes were used:

- YBCO on $LaAlO_3$ substrates
- YBCO/buffer layers/Ni

Direct measurement of the transverse resistivity of striated YBCO/LaAlO samples covered by normal metal layer

The aim of the following experiments is to demonstrate the importance of the boundary resistivity, ρ_b, on the resistivity in the direction parallel and perpendicular (transverse) to the filament axis. The measured sample is S 222.2, the filaments were covered by 0.5 micron thick continuous Ag layer, as shown in Fig.4.4.3.

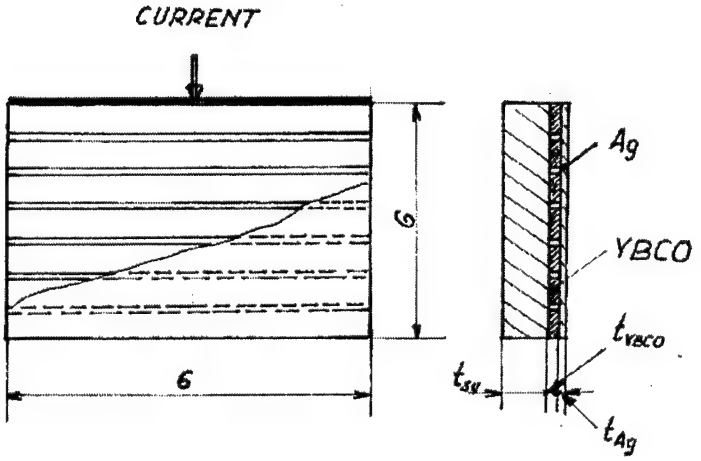

Fig. 4.4.3

The total resistance between 2 points across the filamentary tape, proportional to transverse resistivity, can be determined as:

$$R_{12} = (R_f + R_g)\, N_f \sim \rho_{tr} \qquad (1)$$

where R_f is the resistance of the section containing the filament shunted by Ag layer which are joined via the boundary layer with resistivity ρ_b, R_f is the resistance of Ag layer between two filaments, N_f is the number of filaments between points 1 and 2.
The resistance R_f is strongly affected by ρ_b. Due to finite value of it only a part of the current I flows into the filament and back.

The resistance R_{Ag} is

$$R_{Ag} = N_f\, \rho_{Ag}\, [2g/(t_{Ag}\, w)] \qquad (2)$$

where ρ_{Ag} and t_{Ag} is the resistivity and thickness of Ag layer, w is the sample width, 2g is the gap width.

We measured the same sample with 2 different systems of current and potential contacts, as shown in Fig. 4.4.4. a and b. After these measurements the sample was processed in O_2 atmosphere at 350°C 20 minutes and the measurements were made again.
It is clear that in the case of a good contact YBCO/Ag the sample should exhibit zero resistance and the resistance in the case b is proportional to ρ_{tr}.

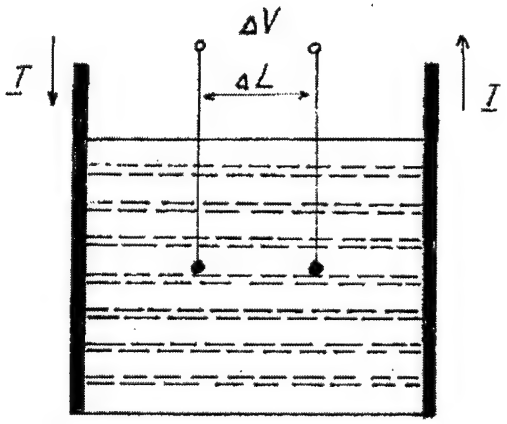

Fig.4.4.4.a

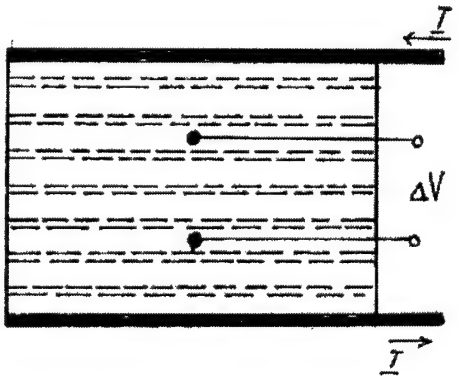

Fig.4.4.4.b

The results of the measurements are given in the following tables.

T1: Current flowing parallel to the filament axis, sample as received, ΔL=2.5 mm

I (mA)	$\Delta V_{(300K)}$ (μV)	$R_{(300K)}$ (Ω)	$R_{11(300K)}$ (Ω)	$\Delta V_{(77K)}$ (μV)	$R_{(77K)}$ (Ω)	$R_{11(77K)}$ (Ω)	$R_{11(77K)}/R_{11(300K)}$
10	95.6	9.56×10^{-3}	1.91×10^{-2}	42	4.2×10^{-3}	8.36×10^{-3}	0.44
20	190.7	9.54×10^{-3}	1.91×10^{-2}	83.6	4.18×10^{-3}	4.18×10^{-3}	0.439

T2: Current flowing parallel to filament axis, sample annealed in O_2 20 minutes, 350^0C

I (mA)	$\Delta V_{(300K)}$ (μV)	$R_{(300K)}$ (Ω)	$R_{11(300K)}$ (Ω)	$\Delta V_{(77K)}$ (μV)
5	53.4	1.07×10^{-2}	1.48×10^{-2}	0
10	107.5	1.08×10^{-2}	1.5×10^{-2}	0

15	161.1			0
20	215			0

T3: Current flowing perpendicular to filament axis, sample as received, ΔL=1.7 mm

I (mA)	$\Delta V_{(300K)}$ (μV)	$R_{(300K)}$ (Ω)	$R_{11(300K)}$ (Ω)	$\Delta V_{(77K)}$ (μV)	$R_{(77K)}$ (Ω)	$R_{11(77K)}$ (Ω)	$R_{11(77K)}/R_{11(300K)}$
10	29.1	2.91×10^{-3}	1.03×10^{-2}	13.4	1.34×10^{-3}	4.73×10^{-3}	0.461
20	58.7	2.94×10^{-3}	1.04×10^{-2}	27.1	1.36×10^{-3}	4.80×10^{-3}	0.462

T4: Current flowing perpendicular to filament axis, sample annealed 350^0/20 min, ΔL=2.5 mm

I (mA)	$\Delta V_{(300K)}$ (μV)	$R_{(300K)}$ (Ω)	$R_{11(300K)}$ (Ω)	$\Delta V_{(77K)}$ (μV)	$R_{(77K)}$ (Ω)	$R_{11(77K)}$ (Ω)	$R_{11(77K)}/R_{11(300K)}$
10	45.7	4.57×10^{-3}	1.1×10^{-2}	6.0	6×10^{-4}	1.5×10^{-3}	0.132
20	90.9	4.55×10^{-3}	1.1×10^{-2}	16.0	8×10^{-4}	1.9×10^{-3}	0.176

4.5. Measurements of samples obtained from Dayton laboratories (Dr. Nekkanti Rama)

The Hall probe technique was used to investigate the behaviour of magnetic field in the vicinity of the measured sample. Cu magnet is used to generate external AC magnetic field directed perpendicularly to the surface of the tape.

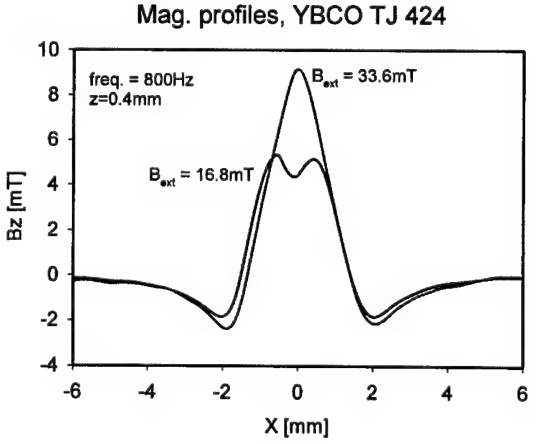

Fig. 4.5. 1 Magnetic profiles of B_z – component for external field of frequency

The measuring and compensation Hall probes are used to generate signal relative to the magnetic field. The measuring cards are used for data acquisition.

1. Magnetic profiles of B_z - component above YBCO TJ 424 (monocore) tape were measured for different amplitudes and frequencies of external magnetic field.

Two profiles at the frequency 800Hz, 0.4mm above the sample can be seen on the **fig. 1**. The two curves correspond to different amplitudes of external magnetic field 16.8mT and 33.6mT.

Conclusion:

- with increasing of frequency, current flowing inside the sample is expelled to the edges, thus causing skin-effect like behaviour.

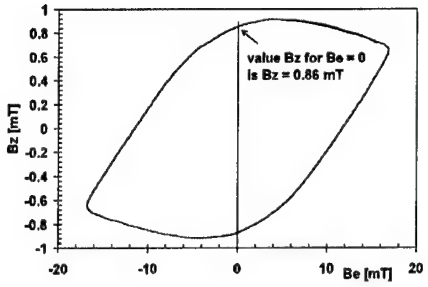

Fig. 5.4.2 Explanation of construction of 1 point of frequency characteristics.

2. The hysteresis loops above the central point of the sample for various frequencies were measured to find out the frequency response.
Thus the frequency characteristics was made out from the loops in the way described in the fig.5.4.2.

In Fig. 5.4.3, the "width" of hysteresis loop as a function of frequency is plotted (or frequency as a function of loop's "width", respectively).

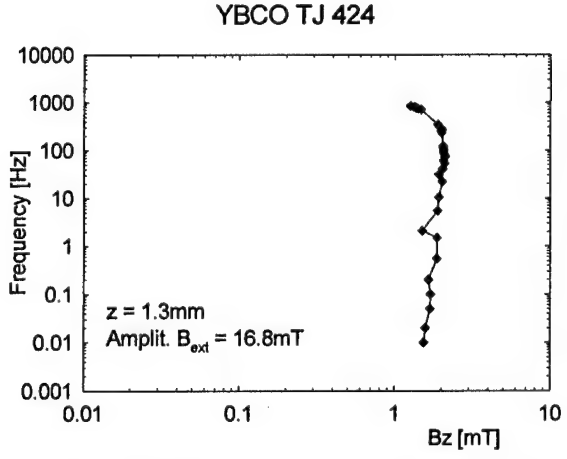

Fig. 5.4.3 Frequency dependence of width of the hysteresis loop

As the frequency is a measure of induction voltage, hence electric field, by means of equations (1, 2);

$$u_i = -\frac{d\Phi(t)}{dt} = -A\frac{dB(t)}{dt} \qquad (1)$$

$$u_i = \int_C E.dr \qquad (2)$$

magnetic flux density B_z is a measure of current amplitude, we can calculate quasi Current – Voltage relation using the following expressions:

$$I = \frac{2.5.10^6.wf}{\ln\left(\frac{\sqrt{z^2 + wf^2}}{z}\right)}.B_z \qquad (3)$$

$$E = \frac{2.\pi.A.B_{ext}}{r}.f \qquad (4)$$

Where z is height above the sample, wf is half width of the sample; A is area of the surface, r is outer circumference of the sample.

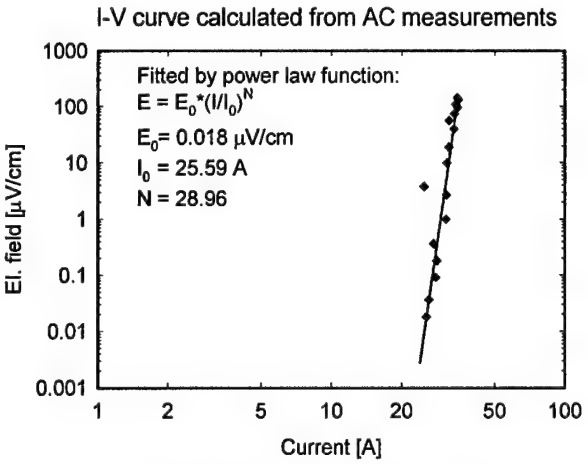

Fig.5.4. 4 Quasi Current – Voltage relation in log-log scale.

In Fig. 5.4.4, the calculated quasi I-V curve in log–log scale is shown.

Conclusions:

- from Fig. 5.4.3, one can see a qualitative distortion of a shape of I-V curve that was expected to obey power law, hence to be linear in log-log scale. This can be explained by the skin-effect behaviour in region above 80Hz for amplitudes round 16.8 mT, which do not seem to be enough to penetrate whole sample within frequency range up to 800 Hz.

- the power law can be used for the data up to 80 Hz

- data were fitted by power law function:

$$E = E_0.\left(\frac{I}{I_0}\right)^N \qquad (5)$$

a) we chose two parameters: $E_0 = 0.018$ μV/cm, $I_0 = 25.59$ A
b) fitted parameter $N = 28.96$

- critical current estimate was realized according to the equation:

$$I_c = I_0 \cdot \left(\frac{E}{E_0} \right)^{(1/N)} \qquad (6)$$

using 1 μV/cm criterion we get $I_c = 29.4$ A

- for the future measurements, higher amplitudes of external magnetic field are needed! Values 30 mT and more seem to be sufficient.

5. Measurement set-ups for AC loss measurements

The effect of coupling currents can be also studied by measuring the total losses of the tape and separating the hysteresis and coupling losses. The main problem of a measuring set up for loss measurements is the low loss level, in particular for the case of striated samples with narrow filaments. We tested several methods, as mentioned in the first part of the report. In the following we describe two measuring set-ups, which are under development in the frame of this project.

5.1. Measuring system with lock-in amplifier

1-Description of the system.

The system consists of a pick-up coil (PC) and a compensation coil (CC). A measured sample is placed into PC. When a sample is subjected to an AC external magnetic field, the magnetization currents are induced in the sample, giving rise to an AC magnetic moment M of the sample. In the case of an YBCO multifilamentary sample covered by a normal metal layer, its magnetic moment consists of two components, i.e.: M = Mh + Mcc, where Mh is due to the magnetization of the filaments, while Mcc is due to the coupling currents. The time dependent voltage difference U(t) = U(PC) - U(CC) is proportional to dM/dt.The detailed and an appropriate analysis of the measured voltage difference U(t) provides the informations about the properties of the sample: losses, critical sheet current Ic[A/m] and time constant of the coupling currents TAU ~ 1/ROeff, where ROeff is an effective matrix resistivity.

2-Theory

When an Lock-in amplifier is used for measurements, one obtains two voltage amplitudes:1Ur and 1Ui, i.e., the real (resistive) and the imaginary (inductive) part of the first harmonic 1U(t) of the measured voltage U(t). Both 1Ur and 1Ui themselves consist of two components:

1Ur = 1Urh + 1Urcc, ...(1)

1Ui = 1Uih + 1Uicc, ...(2)

where 1Urh and 1Uih are due to the filament magnetization (they are proportional to dMh/dt, while 1Urcc and 1Uicc are due to the coupling currents (they are proportional to dMcc/dt). For an appropriate interpretation and analysis of the measured 1Ur and 1Ui one needs to determine all four quantities appearing in (1) and (2) from the experimental data obtained for 1Ur and 1Ui. This can be done by using the theoretical expressions for them. They were derived using the existing theories for filament magnetization and coupling currents. As a first step we derived the solulion for the time dependent voltage difference U(t) = Uh(t) + Ucc(t) in an analytical form (here Uh(t) and Ucc(t) denote, as before, the filament magnetization component and coupling current component respectively. It is also worth to note here, that for a harmonic external magnetic field B(t) the component Ucc(t) is also harmonic whill Uh(t) is not). Subsequently, the Fourier transform was used to derive the solution for the first harmonic 1U(t) and the expressions for the amplitudes 1Ur and 1Ui in the form as given above by (1) and (2).

2.1- The most important properties of the derived solutions:

a)- Coupling current components are the functions of the frequency f, they are linear in field amplitude Bo and do not depend on critical sheet current Ic. For the frequencies f < 0.2fc (where the characteristic frequency fc = 1/6.28TAU) they are proportional to TAU, i.e., they are inversely proportional to the effective matrix resistivity ROeff for given f and Bo. Under this condition 1Urcc ~ f^2, and 1Uicc ~ f^3. For f >> fc, the component 1Urcc saturates (its frequency dependence becomes very weak). >>>

b)- Components due to filamentary magnetization are linear in frequency f, but their field amplitude dependence is rather complicated and is strongly influenced by the critical sheet current Ic. On the other hand, for Bo < 0.4Bc (where the characteristic field Bc = 4.10^-7*Ic [T]), then 1Urh ~ Bo^3, and 1Uih becomes linear in Bo. It must be emphasized here, that since the theoretical solutions were derived for Ic = const (i.e.,Ic does not depend neither on B, nor on dB/dt), they are not valid for large field amplitude Bo >> Bc. For this reason the measurements should be performed for Bo comparable with Bc or smaller than Bc. In this range of Bo the assumption Ic = const is justified and an average value of Ic can be obtained from the experimental data for 1Urh and for 1Uih.

2.2- Concluding remark:

On the basis of the above mentioned features of the theoretical solutions one may conclude, that the most convenient conditions for evaluation of the effective matrix resistivity ROeff from the experimental data are fulfilled for field amplitude Bo < 0.4Bc and frequency f < 0.2fc.

3- Experimental verification of the theoretical results.

Two samples (A and B) were used for the experimental verification of the theoretical results:

3.1- Sample A:

This sample is just a short circuited loop made of a copper wire. The loop has the form of a rectangle 4*40mm^2. The current induced in this loop simulates the coupling currents in a real multifilamentary conductor covered by a normal metal layer. Since all necessary parameters of this sample are known, the components 1Urcc and 1Uicc can be calculated exactly and compared with the measured data. (For this sample 1Urh = 1Uih = 0).The agreement between the experimental and theoretical results was found to be very good for all Bo and f used for measurements (field amplitude Bo ranged from 0.2mT to 1.5mT and frequency from 30Hz to 9000Hz).

3.2- Sample B:

This sample is an YBCO strip on a ceramic substrate and covered by a thin Au layer of a fraction of micron in thickness. (Sample width: 4.5mm, sample length: 40 mm). Contrary to the sample A, here 1Urcc = 1Uicc =0, since the coupling currents are absent. Measurements were performed for field amplitudes Bo ranging from 0.2mT to 8mT with frequencies 40Hz, 53Hz and 103Hz. Very good agreement was found for the measured and calculated component 1Uih. The average critical sheet current was obtained from the fit, and was found to be Ic = 8833A/m (Bc = 3.53mT). Somewhat worse agreement was obtained for the component 1Urh (but still acceptable for 53Hz). The data are scattered probably due to very small 1Urh (fractions of microvolt for small Bo). It is believed, that this will be improved by using a new set of PC and CC (ready for testing), which should give the voltages of two orders of magnitude larger.

5.2 Evaluation of AC losss in high Tc superconducting tapes using Fourier analysis

1. Introduction

The experimental apparatus for the measurement of magnetisation curves and evaluation of ac power losses is further described. The aim was the testing of equipment devoted to the measurement of magnetisation curves of thin strip samples made of HTc superconductors within the frequency range up to ~1000 Hz required by the intended applications of the materials under investigation.

2. Experimental set-up

The block diagram of experimental equipment is shown in Fig. 5.2.1. As a source of magnetic field with defined field strength waveform a long copper wire solenoid coil driven by the power current source along with signal generator was used.

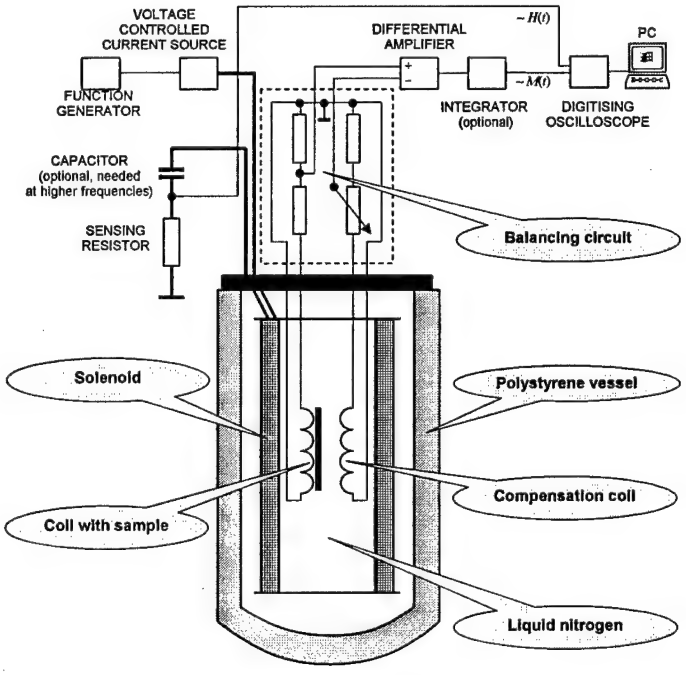

Fig. 5.2.1 The block diagram of experimental equipment.

The sample (thin strip) is positioned in such a way that the exciting magnetic field vector is perpendicular to the strip plane. To increase the maximum applicable current at higher frequencies (limited by the loading impedance increasing with frequency and maximum output voltage of the current source) a capacitor should be connected in series with the sensing resistor and solenoid inductance. Thus, the series resonance circuit is created allowing the voltage drop across the inductor and/or capacitor to be higher than the maximum output voltage provided by the current source. In case of capacitor usage the care must be taken with regard to the breakdown voltage of the capacitor and proper coil wire isolation, since the voltage across the capacitor and inductor in the resonant state is much higher than the total voltage across the resonant circuit due to relatively high quality factor.

The voltage used for determining the magnetic moment was measured using differential pick-up coils. The sample was inserted in the vicinity of one coil meanwhile the second coil was used for the compensation of the air flux. The pick-up coil system was placed into the solenoid and immersed into liquid nitrogen.

Two types of balancing circuits were used for minimising (zeroing) output signal without sample. The first was a relatively simple passive resistive circuit made of two voltage dividers – one with constant and one with variable division ratio. The main disadvantage is that the pick-up coils are loaded by the total resistance of dividers what might result in signal distortion. Another constraint is that the variable divider should be connected to the compensation coil only; otherwise the overall calibration constant changes slightly as the balancing is carried out. The second advanced type of active balancing circuit uses two high-performance non-inverting operational amplifiers to separate the pick-up coils from the rest of equipment. The balancing is performed by means of changing the gain of the amplifier connected to the compensation coil. The gain of amplifier connected to the coil with the sample must be known and kept constant to keep away from changes of calibration constant. Thanks to very high input impedance the coils behave like unloaded (open-circuit), thus there is no above mentioned signal distortion. The experiments shown very good properties of balancing circuit – the only disadvantage appears at high frequencies, where the pick-up coil signal connected to the inputs can reach the magnitude of the supply voltage of the operational amplifiers resulting in the signal limitation and distortion. This problem can easily be avoided either by proper design of pick-up coils (decreasing the number of turns or the cross-sectional area) or (worse case) using attenuators at the inputs of balancing circuits.

Using any of the balancing circuits, the differential output voltage is only proportional to the time derivative of total sample magnetic moment (or magnetisation), because the common mode voltage is eliminated. Further amplification is carried out by means of differential instrumentation amplifier with properly adjusted gain with regard to the frequency and full-scale sensitivity of digital oscilloscope. Both the voltage drop across the sensing resistor (proportional to the magnetising field strength) and the induced voltage are sampled by the digital storage oscilloscope. The output signal of pick-up coils is integrated either by an electronic integrator or numerically to obtain magnetic moment (or magnetisation) waveform. The advantages and disadvantages of both methods were discussed e.g. in [1, 2]. For low frequencies the numerical integration appears to be more convenient mainly because of integrator drift elimination, at high frequencies the phase errors of analogue integrators could become significant. For the numerical integration the trapezoidal method was used since it appeared to be the simplest and fastest method for these purposes; nevertheless any integration algorithms built-in commercially available instrumentation software (such as LabView, Agilent VEE, etc.) can be used.

Thus, the magnetisation curves (magnetic moment versus the exciting magnetic flux density) are measured.

3. Calibration procedure

The magnetic field magnitude as a function of exciting current was calibrated using the Hall sensor placed in and moved along the longitudinal solenoid axis to verify the location of homogeneous field region.

An extra effort has been devoted to precise calibration of pick-up coils. The output signal is affected by various sources of stray fields. This influence cannot be estimated easily, so that the calibration was performed by means of the measurement of known magnetic moment. As the source of known magnetic moment either a rectangular single-turn coil surrounding known area or a two-strip flat wire unit driven by known current have been used. In both cases the magnetic moment can easily be calculated from the definition formula assuming known dimensions and driving current, so that the calibration can be accomplished in a relatively simple way. A

complication is a different magnetic field deformation in the vicinity of each magnetic moment source causing unpredictable results depending on spatial distribution of local magnetic moments within pick-up coil central region. For this reason the sample must be placed in a sufficient distance from the pick-up coil central plane. This effect is demonstrated in Fig. 2 where the influence of the distance on the measured ratio of the magnetic moments of both coil and flat wire is shown.

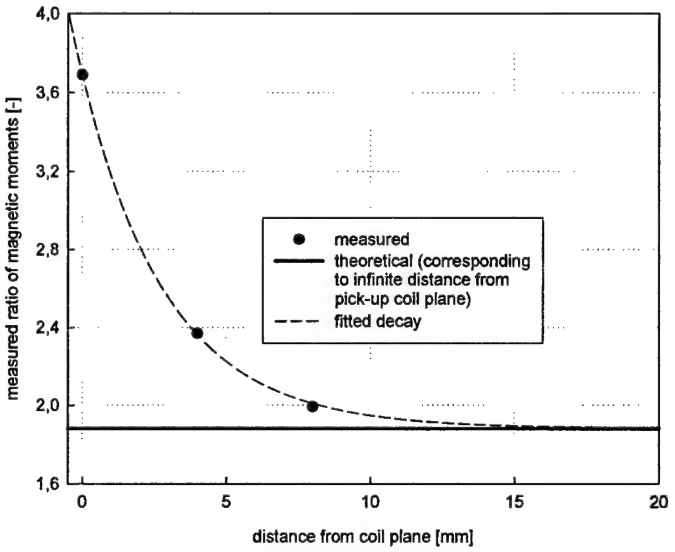

Fig. 5.2.2. The measured and theoretical ratio of magnetic moments versus the distance from the central plane of pick-up coils.

One can see that the increasing the distance from the pick-up coil plane the measured ratio of magnetic moments approaches theoretical value calculated from known parameters of the single-turn coil and two-strip flat wire samples – local field deformations become negligible far from the sources. Thus, assuming a sufficient distance from the central plane, the signal level should be proportional to the total magnetic moment of the sample regardless of its shape and inner arrangement (number and placing of filaments within the tape, inter-filament coupling, etc.). On the other hand the induced voltage level radically falls, so that the compromise must be find between increasing the distance resulting in induced voltage decrease.

After the calibration constant of the pick-up coils was found, additional calibration experiments, focused on direct ac power loss measurements have been carried out. Again, two model samples with the power losses to be easily calculated from known sample dimensions and specific resistance were used. The first was a sample made of single silver strip, in which the ac power losses correspond to eddy-current losses. The eddy current losses p_{eddy} per unit length of such a sample can be estimated using classical Steinmetz theory as

$$p_{eddy} = \frac{\pi^2 \cdot f^2 \cdot B_m^2 \cdot \tau \cdot w^3}{6 \cdot \rho} \qquad (1)$$

where f is the frequency, B_m is the exciting magnetic flux density magnitude, τ is the sample thickness, w is the sample width and ρ is the specific resistance of the sample material. The resistance was measured by means of 4-

wire method. The comparison between measured and calculated losses is shown in Fig. 3. One can see very good agreement between measured and calculated values regardless of frequency and exciting field values.

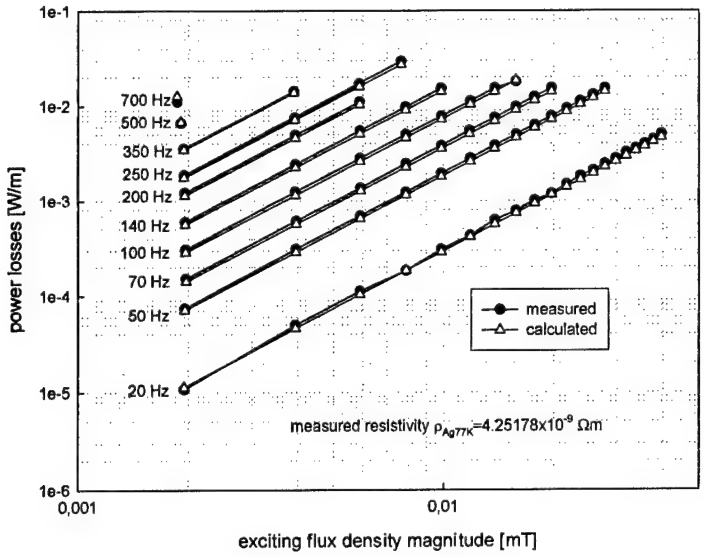

Fig. 5.2.3 The comparison of measured and calculated power losses per unit length versus the flux density magnitude at various frequencies, Ag strip sample 59x4x0.3 mm^3, temperature 77K, sinusoidal exciting field.

The second type of model sample was a single-turn short-circuited coil. In this case the power losses p per unit length can be easily calculated as

$$p = \frac{4 \cdot \pi^2 \cdot f^2 \cdot B_m^2 \cdot w^2 \cdot l}{2 \cdot R} \tag{2}$$

where l is the sample length and R is the total resistance of the coil wire. Note that this formula is valid only in low-frequency region, where the imaginary component of coil impedance (associated with the inductance) can be neglected. The inductance of the rectangle made of round wire is

$$L = \frac{\mu_0}{\pi}\left[x \cdot \ln\left(\frac{2x}{r}\right) + y \cdot \ln\left(\frac{2y}{r}\right) + 2 \cdot \sqrt{x^2 + y^2} - x \cdot \sinh^{-1}\left(\frac{x}{y}\right) - y \cdot \sinh^{-1}\left(\frac{y}{x}\right) - 1.75 \cdot (x + y)\right] \tag{3}$$

where r is the wire radius, x and y are the rectangle side lengths, μ_0 is the vacuum permeability, [3]. For given coil dimensions and the frequency range of interest the influence of the inductance is in fact negligible. The comparison between measured and calculated losses is shown in Fig. 5.2.4.

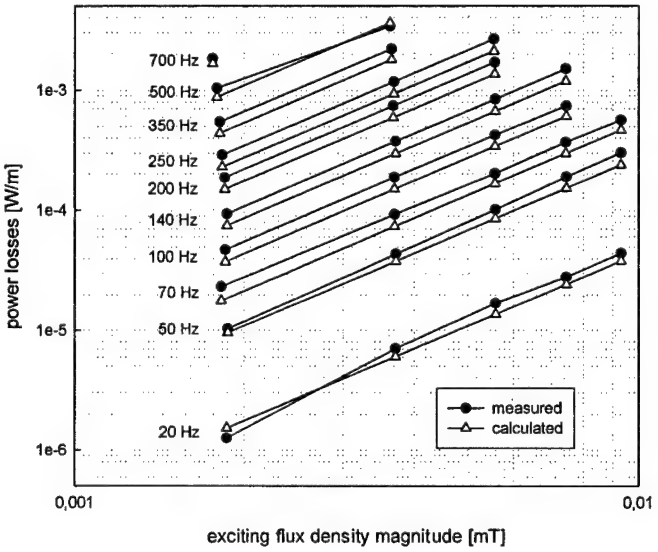

Fig. 5.2.4. The comparison of measured and calculated power losses per unit length versus the flux density magnitude at various frequencies, Cu single-turn sample 60x4x0.4 mm^3, room temperature (298K), sinusoidal exciting field.

4. Power loss evaluation methods

The power losses were evaluated from the obtained magnetisation curves by two ways - conventionally by calculating magnetisation loop area using a simple algorithm (found in [4, 5]) for the calculation of the area of a polygon given by the set of measured loop data points. The algorithm is based on the fact that the area of the triangle with two sides corresponding to the vectors is equal to one half of the absolute value of the vector product of given vectors. Since any polygon can be dissected to the set of triangles, the total area can be found as a summation of corresponding triangle areas.

Power losses (related to one cycle and the unit of length) can be calculated from the magnetisation curve area A as (f – frequency, l – sample length)

$$p = \frac{A \cdot f}{l} \tag{4}$$

The second method used the discrete Fourier transform (DFT) for the calculation of the amplitude and phase spectra of the magnetising flux density and magnetic moment waveforms respectively, see i.e. [6]. The spectra of both waveforms consist of ~N/2 harmonic components (N is number of points per one waveform period). The complex power s_n of n-th harmonic component (for n>0) related to unit strip length can be calculated as

$$s_n = p_n + jq_n = \frac{n\,\pi\,f\,B_{mn}\,m_{mn}}{l_s} \exp\left[j\left(\varphi_{Bn} - \varphi_{mn} + n \cdot \frac{\pi}{2} \right) \right] \tag{5}$$

where B_{mn} is the magnitude of n-th harmonic of the flux density, φ_{Bn} is the phase angle of n-th harmonic of the flux density, m_{mn} is the magnitude of n-th harmonic of the magnetic moment and φ_{mn} is the phase angle n-th harmonic of the magnetic moment. The contribution of each harmonic component (the real part of the complex power) to the total power losses is

$$p_n = \frac{n\,\pi\,f\,B_{mn}\,m_{mn}}{l_s} \cos\left(\varphi_{Bn} - \varphi_{mn} + n \cdot \frac{\pi}{2} \right) \tag{6}$$

The total power losses are given by the sum of all the contributions:

$$p_{DFT} = \sum_{n=1}^{N/2} p_n \tag{7}$$

The power losses calculated from experimentally found magnetisation curves using formulae (4) and (7) exhibit very good agreement to at least 4 significant digits. The advantage of using DFT is that except for the power losses also the reactive and complex or apparent power can be evaluated that can sometimes be interesting from theoretical point of view (similarly to the complex susceptibility and/or permeability in some relevant cases). Moreover it allows calculation of the total harmonic distortion of driving magnetic field directly from the definition

formula thus allowing to reveal the influence of higher harmonic components to the experimental results.

5. Experimental results

Introductory experiments on Bi-2223/Ag and YBCO based samples have been performed too. The first measurements on the equipment showed promising results and functionality. An example of the measured magnetisation curves is shown in Figs. 5 and 6. YBCO-based sample has been used for the experiment. In Figs. 7 and 8 the measured power losses per unit of strip length with respect to the magnetising flux density magnitude and frequency are shown.

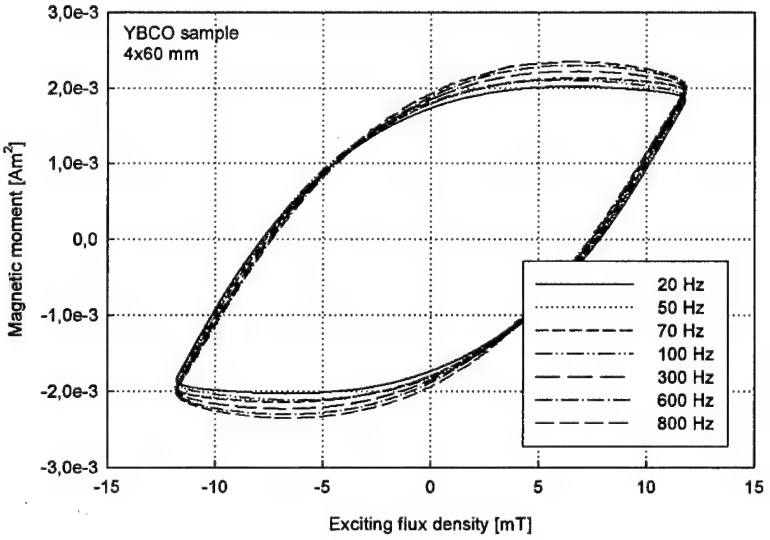

Fig. 5. The example of magnetisation curves at various frequencies, sinusoidal exciting flux density, magnitude 11.82 mT.

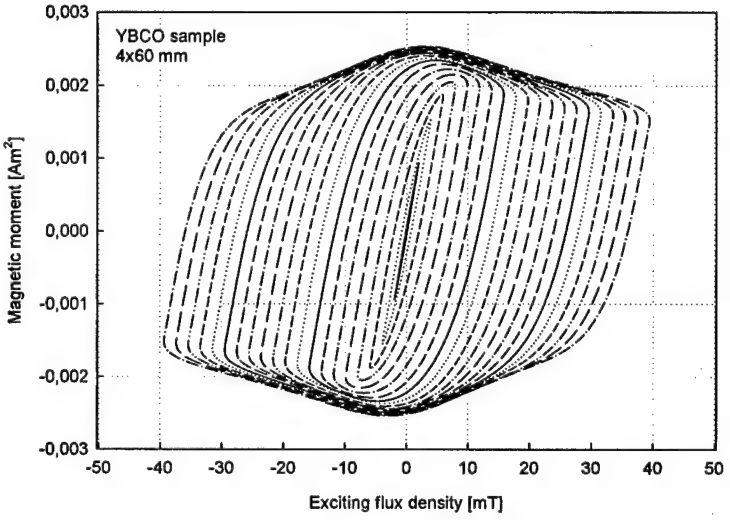

Fig. 6. The example of magnetisation curves at various exciting flux densities (from 1.97 to 39.4 mT, step 1.97 mT), frequency 300 Hz, sinusoidal exciting field.

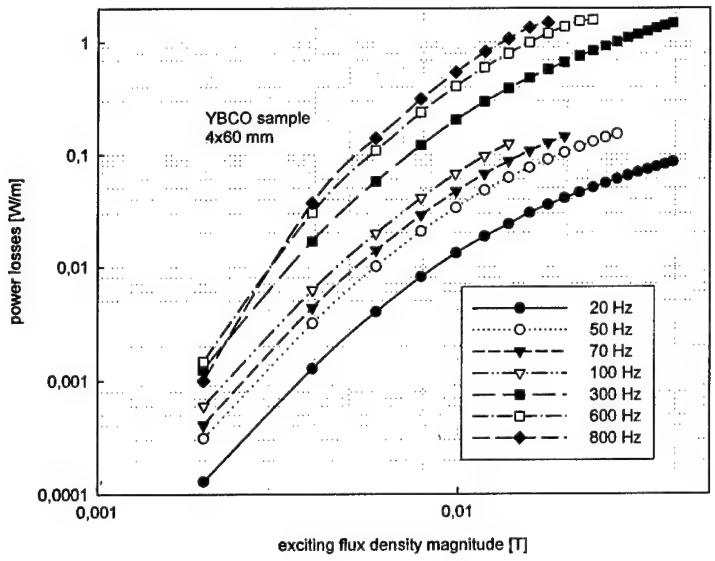

Fig. 7. Power losses versus the magnetising flux density magnitude at various frequencies, sinusoidal exciting field, YBCO sample 4x60 mm.

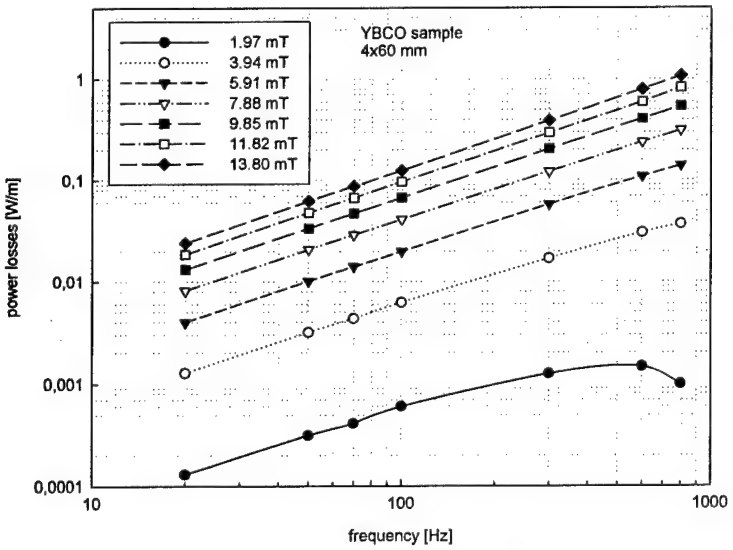

Fig. 8. Power losses versus the frequency at various magnetising flux density magnitudes, sinusoidal exciting field, YBCO sample 4x60 mm.

References:

[1] Ušák, E., Jančárik, V.: Computer-Controlled Hysteresisgraph for Measurement with Arbitrary Signal Waveform, Proceedings of Magnetic Measurements 2000 Conference, Prague, Czech Republic (2000) 33-36
[2] Ušák, E.: Performance Testing of Quasi-Static Digital Hysteresisgraph, Proceedings of the 4th Japan-Central Europe Joint Workshop on Energy and Information in Non-Linear Systems, Brno, Czech Republic (2001) 194-197
[3] Grover, W. F.: Inductance Calculations: Working Formulas and Tables, Dover Publications, Inc., New York, (1946) 60
[4] O'Rourke, J: Computational Geometry in C', Chapter 1, Cambridge Press, (1995).
[5] http://www.brunel.ac.uk/~castjjg/java/polygon/polygon.html.
Ušák, E., Jančárik, V.: Journal of Electrical Engineering **50** (1999) 66-68.

6. Conclusions

Several types of striated samples were prepared and tested.
The transverse resistivity, ρ_{tr}, of samples of striated (filamentary) YBCO tapes prepared within this project very strongly depends on the quality of YBCO/metal layer boundary (stabilizer), characterized by the boundary resistivity, ρ_b, and on the resistivity of this metallic layer.
In samples "as received" the boundary YBCO/metal had quite high resistivity and the shunting effect of the metal was practically negligible. We have found that the heat treatment in O_2 atmosphere improves the boundary properties considerably.
We developed methods to direct as well as indirect determination of the transverse resistivity, based on the measurement of coupling losses.

Declarations

The contractor, Institute of Electrical Engineering, Department of Electrodynamic of Superconductors, hereby declares that, to the best of its knowledge and belief, the technical data delivered herewith under contract F61775-02-W4065, SPC 02-4065
is complete, accurate and complies with all requirements of the contract.

"I certify that there were no subject inventions to declare as defined in FAR 52.227/12, during the performance of this contract."

Date: August 28, 2003
Name and Title of Authorized official: Dr. Milan Polak

Fig. 4.4.3

The total resistance between 2 points across the filamentary tape, proportional to transverse resistivity, can be determined as:

$$R_{12} = (R_f + R_g)\, N_f \sim \rho_{tr} \qquad (1)$$

where R_f is the resistance of the section containing the filament shunted by Ag layer which are joined via the boundary layer with resistivity ρ_b, R_f is the resistance of Ag layer between two filaments, N_f is the number of filaments between points 1 and 2.
The resistance R_f is strongly affected by ρ_b. Due to finite value of it only a part of the current I flows into the filament and back.

The resistance R_{Ag} is

$$R_{Ag} = N_f\, \rho_{Ag}\, [2g/(t_{Ag}\, w)] \qquad (2)$$

where ρ_{Ag} and t_{Ag} is the resistivity and thickness of Ag layer, w is the sample width, 2g is the gap width.

We measured the same sample with 2 different systems of current and potential contacts, as shown in Fig. 4.4.4. a and b. After these measurements the sample was processed in O_2 atmosphere at 350°C 20 minutes and the measurements were made again.
It is clear that in the case of a good contact YBCO/Ag the sample should exhibit zero resistance and the resistance in the case b is proportional to ρ_{tr}.

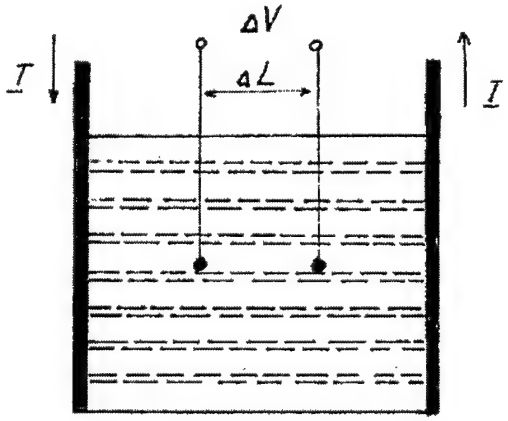

Fig.4.4.4.a

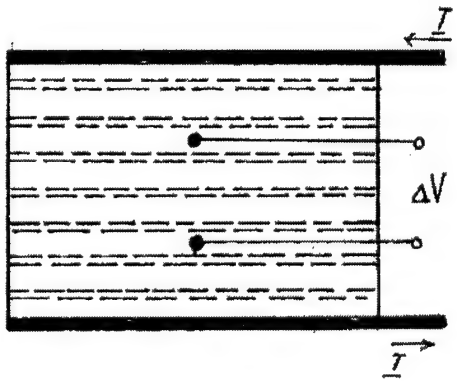

Fig.4.4.4.b

The results of the measurements are given in the following tables.

T1: Current flowing parallel to the filament axis, sample as received, ΔL=2.5 mm

I (mA)	$\Delta V_{(300K)}$ (μV)	$R_{(300K)}$ (Ω)	$R_{11(300K)}$ (Ω)	$\Delta V_{(77K)}$ (μV)	$R_{(77K)}$ (Ω)	$R_{11(77K)}$ (Ω)	$R_{11(77K)}/R_{11(300K)}$
10	95.6	9.56×10^{-3}	1.91×10^{-2}	42	4.2×10^{-3}	8.36×10^{-3}	0.44
20	190.7	9.54×10^{-3}	1.91×10^{-2}	83.6	4.18×10^{-3}	4.18×10^{-3}	0.439

T2: Current flowing parallel to filament axis, sample annealed in O_2 20 minutes, 350^0C

I (mA)	$\Delta V_{(300K)}$ (μV)	$R_{(300K)}$ (Ω)	$R_{11(300K)}$ (Ω)	$\Delta V_{(77K)}$ (μV)
5	53.4	1.07×10^{-2}	1.48×10^{-2}	0
10	107.5	1.08×10^{-2}	1.5×10^{-2}	0

15	161.1			0
20	215			0

T3: Current flowing perpendicular to filament axis, sample as received, ΔL=1.7 mm

I (mA)	$\Delta V_{(300K)}$ (μV)	$R_{(300K)}$ (Ω)	$R_{11(300K)}$ (Ω)	$\Delta V_{(77K)}$ (μV)	$R_{(77K)}$ (Ω)	$R_{11(77K)}$ (Ω)	$R_{11(77K)}/R_{11(300K)}$
10	29.1	2.91×10^{-3}	1.03×10^{-2}	13.4	1.34×10^{-3}	4.73×10^{-3}	0.461
20	58.7	2.94×10^{-3}	1.04×10^{-2}	27.1	1.36×10^{-3}	4.80×10^{-3}	0.462

T4: Current flowing perpendicular to filament axis, sample annealed 350^0/20 min, ΔL=2.5 mm

I (mA)	$\Delta V_{(300K)}$ (μV)	$R_{(300K)}$ (Ω)	$R_{11(300K)}$ (Ω)	$\Delta V_{(77K)}$ (μV)	$R_{(77K)}$ (Ω)	$R_{11(77K)}$ (Ω)	$R_{11(77K)}/R_{11(300K)}$
10	45.7	4.57×10^{-3}	1.1×10^{-2}	6.0	6×10^{-4}	1.5×10^{-3}	0.132
20	90.9	4.55×10^{-3}	1.1×10^{-2}	16.0	8×10^{-4}	1.9×10^{-3}	0.176

4.5. Measurements of samples obtained from Dayton laboratories (Dr. Nekkanti Rama)

The Hall probe technique was used to investigate the behaviour of magnetic field in the vicinity of the measured sample. Cu magnet is used to generate external AC magnetic field directed perpendicularly to the surface of the tape.

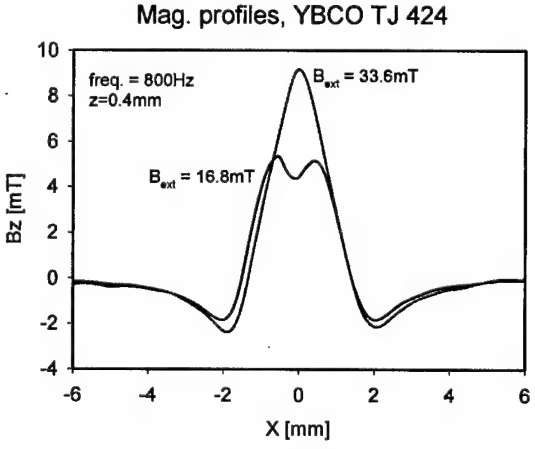

Fig. 4.5. 1 Magnetic profiles of B_z – component for external field of frequency

The measuring and compensation Hall probes are used to generate signal relative to the magnetic field. The measuring cards are used for data acquisition.

1. Magnetic profiles of B_z - component above YBCO TJ 424 (monocore) tape were measured for different amplitudes and frequencies of external magnetic field.

Two profiles at the frequency 800Hz, 0.4mm above the sample can be seen on the **fig. 1**. The two curves correspond to different amplitudes of external magnetic field 16.8mT and 33.6mT.

Conclusion:

- with increasing of frequency, current flowing inside the sample is expelled to the edges, thus causing skin-effect like behaviour.

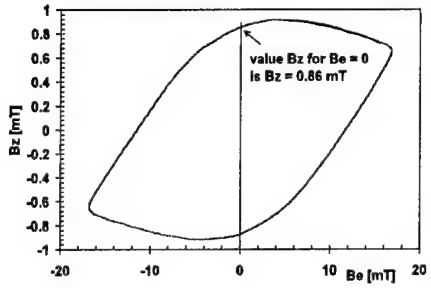

Fig. 5.4.2 Explanation of construction of 1 point of frequency characteristics.

2. The hysteresis loops above the central point of the sample for various frequencies were measured to find out the frequency response.
Thus the frequency characteristics was made out from the loops in the way described in the fig.5.4.2.

In Fig. 5.4.3, the "width" of hysteresis loop as a function of frequency is plotted (or frequency as a function of loop's "width", respectively).

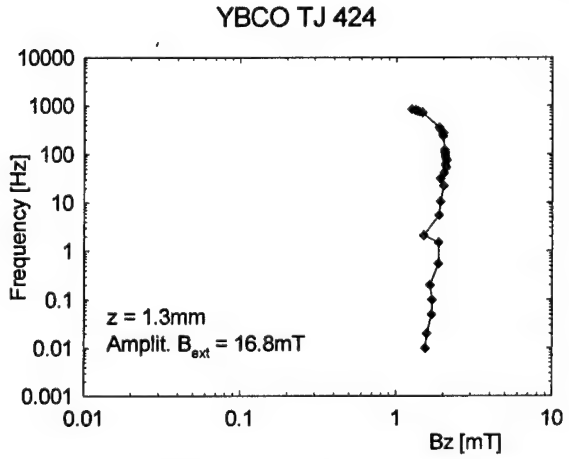

Fig. 5.4.3 Frequency dependence of width of the hysteresis loop

As the frequency is a measure of induction voltage, hence electric field, by means of equations (1, 2);

$$u_i = -\frac{d\Phi(t)}{dt} = -A\frac{dB(t)}{dt} \qquad (1)$$

$$u_i = \int_C E.dr \qquad (2)$$

magnetic flux density B_z is a measure of current amplitude, we can calculate quasi Current – Voltage relation using the following expressions:

$$I = \frac{2.5.10^6.wf}{\ln\left(\frac{\sqrt{z^2 + wf^2}}{z}\right)}.B_z \qquad (3)$$

$$E = \frac{2.\pi.A.B_{ext}}{r}.f \qquad (4)$$

Where z is height above the sample, wf is half width of the sample; A is area of the surface, r is outer circumference of the sample.

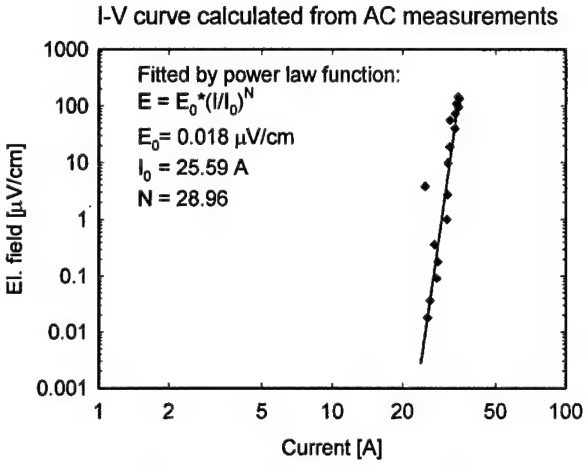

Fig.5.4. 4 Quasi Current – Voltage relation in log-log scale.

In Fig. 5.4.4, the calculated quasi I-V curve in log–log scale is shown.

Conclusions:

- from Fig. 5.4.3, one can see a qualitative distortion of a shape of I-V curve that was expected to obey power law, hence to be linear in log-log scale. This can be explained by the skin-effect behaviour in region above 80Hz for amplitudes round 16.8 mT, which do not seem to be enough to penetrate whole sample within frequency range up to 800 Hz.

- the power law can be used for the data up to 80 Hz

- data were fitted by power law function:

$$E = E_0.\left(\frac{I}{I_0}\right)^N \qquad (5)$$

a) we chose two parameters: $E_0 = 0.018$ μV/cm, $I_0 = 25.59$ A
b) fitted parameter $N = 28.96$

- critical current estimate was realized according to the equation:

$$I_c = I_0 \cdot \left(\frac{E}{E_0} \right)^{(1/N)} \qquad (6)$$

using 1 μV/cm criterion we get $I_c = 29.4$ A

- for the future measurements, higher amplitudes of external magnetic field are needed! Values 30 mT and more seem to be sufficient.

5. Measurement set-ups for AC loss measurements

The effect of coupling currents can be also studied by measuring the total losses of the tape and separating the hysteresis and coupling losses. The main problem of a measuring set up for loss measurements is the low loss level, in particular for the case of striated samples with narrow filaments. We tested several methods, as mentioned in the first part of the report. In the following we describe two measuring set-ups, which are under development in the frame of this project.

5.1. Measuring system with lock-in amplifier

1-Description of the system.

The system consists of a pick-up coil (PC) and a compensation coil (CC). A measured sample is placed into PC. When a sample is subjected to an AC external magnetic field, the magnetization currents are induced in the sample, giving rise to an AC magnetic moment M of the sample. In the case of an YBCO multifilamentary sample covered by a normal metal layer, its magnetic moment consists of two components, i.e.: M = Mh + Mcc, where Mh is due to the magnetization of the filaments, while Mcc is due to the coupling currents. The time dependent voltage difference U(t) = U(PC) - U(CC) is proportional to dM/dt.The detailed and an appropriate analysis of the measured voltage difference U(t) provides the informations about the properties of the sample: losses, critical sheet current Ic[A/m] and time constant of the coupling currents TAU ~ 1/ROeff, where ROeff is an effective matrix resistivity.

2-Theory

When an Lock-in amplifier is used for measurements, one obtains two voltage amplitudes:1Ur and 1Ui, i.e., the real (resistive) and the imaginary (inductive) part of the first harmonic 1U(t) of the measured voltage U(t). Both 1Ur and 1Ui themselves consist of two components:

1Ur = 1Urh + 1Urcc, ...(1)

1Ui = 1Uih + 1Uicc, ...(2)

where 1Urh and 1Uih are due to the filament magnetization (they are proportional to dMh/dt, while 1Urcc and 1Uicc are due to the coupling currents (they are proportional to dMcc/dt). For an appropriate interpretation and analysis of the measured 1Ur and 1Ui one needs to determine all four quantities appearing in (1) and (2) from the experimental data obtained for 1Ur and 1Ui. This can be done by using the theoretical expressions for them. They were derived using the existing theories for filament magnetization and coupling currents. As a first step we derived the solulion for the time dependent voltage difference U(t) = Uh(t) + Ucc(t) in an analytical form (here Uh(t) and Ucc(t) denote, as before, the filament magnetization component and coupling current component respectively. It is also worth to note here, that for a harmonic external magnetic field B(t) the component Ucc(t) is also harmonic whill Uh(t) is not). Subsequently, the Fourier transform was used to derive the solution for the first harmonic 1U(t) and the expressions for the amplitudes 1Ur and 1Ui in the form as given above by (1) and (2).

2.1- The most important properties of the derived solutions:

a)- Coupling current components are the functions of the frequency f, they are linear in field amplitude Bo and do not depend on critical sheet current Ic. For the frequencies f < 0.2fc (where the characteristic frequency fc = 1/6.28TAU) they are proportional to TAU, i.e., they are inversely proportional to the effective matrix resistivity ROeff for given f and Bo. Under this condition 1Urcc ~ f^2, and 1Uicc ~ f^3. For f >> fc, the component 1Urcc saturates (its frequency dependence becomes very weak). >>>

b)- Components due to filamentary magnetization are linear in frequency f, but their field amplitude dependence is rather complicated and is strongly influenced by the critical sheet current Ic. On the other hand, for Bo < 0.4Bc (where the characteristic field Bc = 4.10^-7*Ic [T]), then 1Urh ~ Bo^3, and 1Uih becomes linear in Bo. It must be emphasized here, that since the theoretical solutions were derived for Ic = const (i.e.,Ic does not depend neither on B, nor on dB/dt), they are not valid for large field amplitude Bo >> Bc. For this reason the measurements should be performed for Bo comparable with Bc or smaller than Bc. In this range of Bo the assumption Ic = const is justified and an average value of Ic can be obtained from the experimental data for 1Urh and for 1Uih.

2.2- Concluding remark:

On the basis of the above mentioned features of the theoretical solutions one may conclude, that the most convenient conditions for evaluation of the effective matrix resistivity ROeff from the experimental data are fulfilled for field amplitude Bo < 0.4Bc and frequency f < 0.2fc.

3- Experimental verification of the theoretical results.

Two samples (A and B) were used for the experimental verification of the theoretical results:

3.1- Sample A:

This sample is just a short circuited loop made of a copper wire. The loop has the form of a rectangle 4*40mm^2. The current induced in this loop simulates the coupling currents in a real multifilamentary conductor covered by a normal metal layer. Since all necessary parameters of this sample are known, the components 1Urcc and 1Uicc can be calculated exactly and compared with the measured data. (For this sample 1Urh = 1Uih = 0).The agreement between the experimental and theoretical results was found to be very good for all Bo and f used for measurements (field amplitude Bo ranged from 0.2mT to 1.5mT and frequency from 30Hz to 9000Hz).

3.2- Sample B:

This sample is an YBCO strip on a ceramic substrate and covered by a thin Au layer of a fraction of micron in thickness. (Sample width: 4.5mm, sample length: 40 mm). Contrary to the sample A, here 1Urcc = 1Uicc =0, since the coupling currents are absent. Measurements were performed for field amplitudes Bo ranging from 0.2mT to 8mT with frequencies 40Hz, 53Hz and 103Hz. Very good agreement was found for the measured and calculated component 1Uih. The average critical sheet current was obtained from the fit, and was found to be Ic = 8833A/m (Bc = 3.53mT). Somewhat worse agreement was obtained for the component 1Urh (but still acceptable for 53Hz). The data are scattered probably due to very small 1Urh (fractions of microvolt for small Bo). It is believed, that this will be improved by using a new set of PC and CC (ready for testing), which should give the voltages of two orders of magnitude larger.

5.2 Evaluation of AC losss in high Tc superconducting tapes using Fourier analysis

1. Introduction

The experimental apparatus for the measurement of magnetisation curves and evaluation of ac power losses is further described. The aim was the testing of equipment devoted to the measurement of magnetisation curves of thin strip samples made of HTc superconductors within the frequency range up to ~1000 Hz required by the intended applications of the materials under investigation.

2. Experimental set-up

The block diagram of experimental equipment is shown in Fig. 5.2.1. As a source of magnetic field with defined field strength waveform a long copper wire solenoid coil driven by the power current source along with signal generator was used.

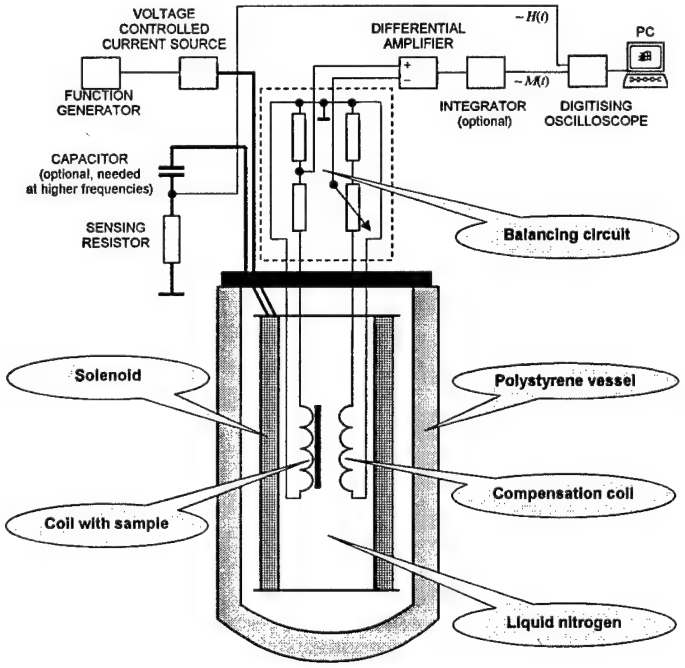

Fig. 5.2.1 The block diagram of experimental equipment.

The sample (thin strip) is positioned in such a way that the exciting magnetic field vector is perpendicular to the strip plane. To increase the maximum applicable current at higher frequencies (limited by the loading impedance increasing with frequency and maximum output voltage of the current source) a capacitor should be connected in series with the sensing resistor and solenoid inductance. Thus, the series resonance circuit is created allowing the voltage drop across the inductor and/or capacitor to be higher than the maximum output voltage provided by the current source. In case of capacitor usage the care must be taken with regard to the breakdown voltage of the capacitor and proper coil wire isolation, since the voltage across the capacitor and inductor in the resonant state is much higher than the total voltage across the resonant circuit due to relatively high quality factor.

The voltage used for determining the magnetic moment was measured using differential pick-up coils. The sample was inserted in the vicinity of one coil meanwhile the second coil was used for the compensation of the air flux. The pick-up coil system was placed into the solenoid and immersed into liquid nitrogen.

Two types of balancing circuits were used for minimising (zeroing) output signal without sample. The first was a relatively simple passive resistive circuit made of two voltage dividers – one with constant and one with variable division ratio. The main disadvantage is that the pick-up coils are loaded by the total resistance of dividers what might result in signal distortion. Another constraint is that the variable divider should be connected to the compensation coil only; otherwise the overall calibration constant changes slightly as the balancing is carried out. The second advanced type of active balancing circuit uses two high-performance non-inverting operational amplifiers to separate the pick-up coils from the rest of equipment. The balancing is performed by means of changing the gain of the amplifier connected to the compensation coil. The gain of amplifier connected to the coil with the sample must be known and kept constant to keep away from changes of calibration constant. Thanks to very high input impedance the coils behave like unloaded (open-circuit), thus there is no above mentioned signal distortion. The experiments shown very good properties of balancing circuit – the only disadvantage appears at high frequencies, where the pick-up coil signal connected to the inputs can reach the magnitude of the supply voltage of the operational amplifiers resulting in the signal limitation and distortion. This problem can easily be avoided either by proper design of pick-up coils (decreasing the number of turns or the cross-sectional area) or (worse case) using attenuators at the inputs of balancing circuits.

Using any of the balancing circuits, the differential output voltage is only proportional to the time derivative of total sample magnetic moment (or magnetisation), because the common mode voltage is eliminated. Further amplification is carried out by means of differential instrumentation amplifier with properly adjusted gain with regard to the frequency and full-scale sensitivity of digital oscilloscope. Both the voltage drop across the sensing resistor (proportional to the magnetising field strength) and the induced voltage are sampled by the digital storage oscilloscope. The output signal of pick-up coils is integrated either by an electronic integrator or numerically to obtain magnetic moment (or magnetisation) waveform. The advantages and disadvantages of both methods were discussed e.g. in [1, 2]. For low frequencies the numerical integration appears to be more convenient mainly because of integrator drift elimination, at high frequencies the phase errors of analogue integrators could become significant. For the numerical integration the trapezoidal method was used since it appeared to be the simplest and fastest method for these purposes; nevertheless any integration algorithms built-in commercially available instrumentation software (such as LabView, Agilent VEE, etc.) can be used.

Thus, the magnetisation curves (magnetic moment versus the exciting magnetic flux density) are measured.

3. Calibration procedure

The magnetic field magnitude as a function of exciting current was calibrated using the Hall sensor placed in and moved along the longitudinal solenoid axis to verify the location of homogeneous field region.

An extra effort has been devoted to precise calibration of pick-up coils. The output signal is affected by various sources of stray fields. This influence cannot be estimated easily, so that the calibration was performed by means of the measurement of known magnetic moment. As the source of known magnetic moment either a rectangular single-turn coil surrounding known area or a two-strip flat wire unit driven by known current have been used. In both cases the magnetic moment can easily be calculated from the definition formula assuming known dimensions and driving current, so that the calibration can be accomplished in a relatively simple way. A

complication is a different magnetic field deformation in the vicinity of each magnetic moment source causing unpredictable results depending on spatial distribution of local magnetic moments within pick-up coil central region. For this reason the sample must be placed in a sufficient distance from the pick-up coil central plane. This effect is demonstrated in Fig. 2 where the influence of the distance on the measured ratio of the magnetic moments of both coil and flat wire is shown.

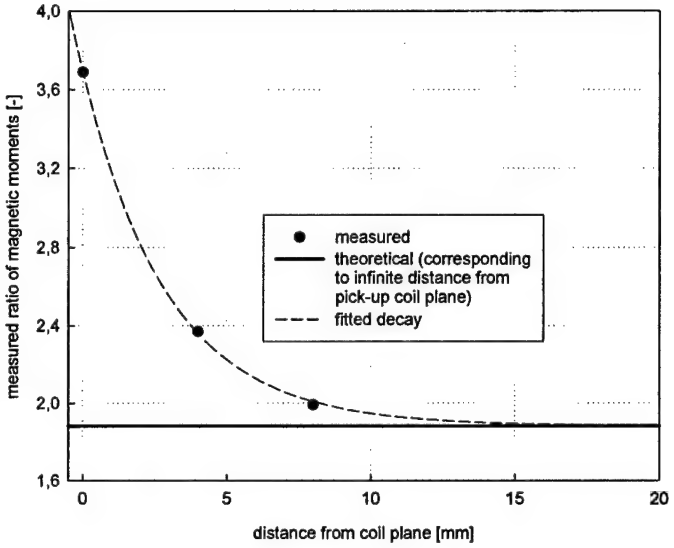

Fig. 5.2.2. The measured and theoretical ratio of magnetic moments versus the distance from the central plane of pick-up coils.

One can see that the increasing the distance from the pick-up coil plane the measured ratio of magnetic moments approaches theoretical value calculated from known parameters of the single-turn coil and two-strip flat wire samples – local field deformations become negligible far from the sources. Thus, assuming a sufficient distance from the central plane, the signal level should be proportional to the total magnetic moment of the sample regardless of its shape and inner arrangement (number and placing of filaments within the tape, inter-filament coupling, etc.). On the other hand the induced voltage level radically falls, so that the compromise must be find between increasing the distance resulting in induced voltage decrease.

After the calibration constant of the pick-up coils was found, additional calibration experiments, focused on direct ac power loss measurements have been carried out. Again, two model samples with the power losses to be easily calculated from known sample dimensions and specific resistance were used. The first was a sample made of single silver strip, in which the ac power losses correspond to eddy-current losses. The eddy current losses p_{eddy} per unit length of such a sample can be estimated using classical Steinmetz theory as

$$p_{eddy} = \frac{\pi^2 \cdot f^2 \cdot B_m^2 \cdot \tau \cdot w^3}{6 \cdot \rho} \qquad (1)$$

where f is the frequency, B_m is the exciting magnetic flux density magnitude, τ is the sample thickness, w is the sample width and ρ is the specific resistance of the sample material. The resistance was measured by means of 4-

wire method. The comparison between measured and calculated losses is shown in Fig. 3. One can see very good agreement between measured and calculated values regardless of frequency and exciting field values.

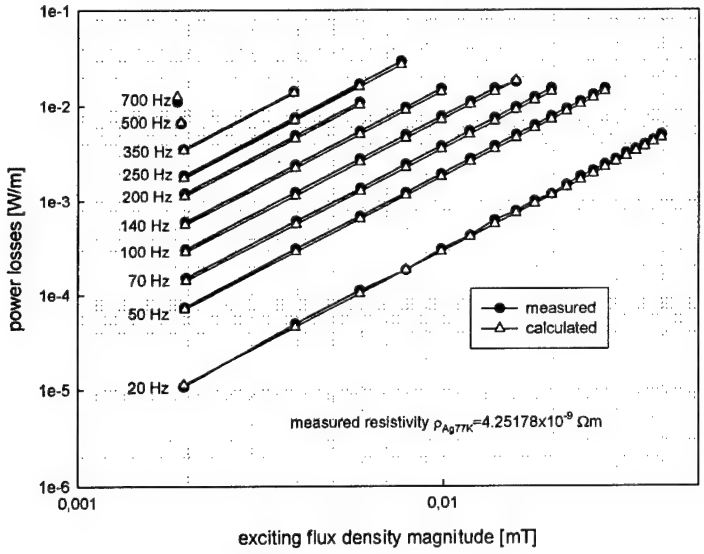

Fig. 5.2.3 The comparison of measured and calculated power losses per unit length versus the flux density magnitude at various frequencies, Ag strip sample 59x4x0.3 mm^3, temperature 77K, sinusoidal exciting field.

The second type of model sample was a single-turn short-circuited coil. In this case the power losses p per unit length can be easily calculated as

$$p = \frac{4 \cdot \pi^2 \cdot f^2 \cdot B_m^2 \cdot w^2 \cdot l}{2 \cdot R} \tag{2}$$

where l is the sample length and R is the total resistance of the coil wire. Note that this formula is valid only in low-frequency region, where the imaginary component of coil impedance (associated with the inductance) can be neglected. The inductance of the rectangle made of round wire is

$$L = \frac{\mu_0}{\pi}\left[x \cdot \ln\left(\frac{2x}{r}\right) + y \cdot \ln\left(\frac{2y}{r}\right) + 2 \cdot \sqrt{x^2 + y^2} - x \cdot \sinh^{-1}\left(\frac{x}{y}\right) - y \cdot \sinh^{-1}\left(\frac{y}{x}\right) - 1.75 \cdot (x + y)\right] \tag{3}$$

where r is the wire radius, x and y are the rectangle side lengths, μ_0 is the vacuum permeability, [3]. For given coil dimensions and the frequency range of interest the influence of the inductance is in fact negligible. The comparison between measured and calculated losses is shown in Fig. 5.2.4.

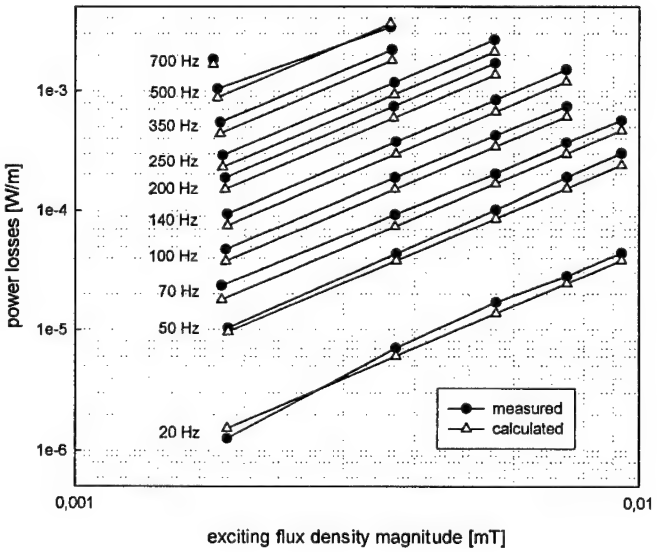

Fig. 5.2.4. The comparison of measured and calculated power losses per unit length versus the flux density magnitude at various frequencies, Cu single-turn sample 60x4x0.4 mm^3, room temperature (298K), sinusoidal exciting field.

4. Power loss evaluation methods

The power losses were evaluated from the obtained magnetisation curves by two ways - conventionally by calculating magnetisation loop area using a simple algorithm (found in [4, 5]) for the calculation of the area of a polygon given by the set of measured loop data points. The algorithm is based on the fact that the area of the triangle with two sides corresponding to the vectors is equal to one half of the absolute value of the vector product of given vectors. Since any polygon can be dissected to the set of triangles, the total area can be found as a summation of corresponding triangle areas.

Power losses (related to one cycle and the unit of length) can be calculated from the magnetisation curve area A as (f – frequency, l – sample length)

$$p = \frac{A \cdot f}{l} \tag{4}$$

The second method used the discrete Fourier transform (DFT) for the calculation of the amplitude and phase spectra of the magnetising flux density and magnetic moment waveforms respectively, see i.e. [6]. The spectra of both waveforms consist of ~N/2 harmonic components (N is number of points per one waveform period). The complex power s_n of n-th harmonic component (for n>0) related to unit strip length can be calculated as

$$s_n = p_n + jq_n = \frac{n\pi f B_{mn} m_{mn}}{l_s} \exp\left[j\left(\varphi_{Bn} - \varphi_{mn} + n \cdot \frac{\pi}{2} \right) \right] \tag{5}$$

where B_{mn} is the magnitude of n-th harmonic of the flux density, φ_{Bn} is the phase angle of n-th harmonic of the flux density, m_{mn} is the magnitude of n-th harmonic of the magnetic moment and φ_{mn} is the phase angle n-th harmonic of the magnetic moment. The contribution of each harmonic component (the real part of the complex power) to the total power losses is

$$p_n = \frac{n\pi f B_{mn} m_{mn}}{l_s} \cos\left(\varphi_{Bn} - \varphi_{mn} + n \cdot \frac{\pi}{2} \right) \tag{6}$$

The total power losses are given by the sum of all the contributions:

$$p_{DFT} = \sum_{n=1}^{N/2} p_n \tag{7}$$

The power losses calculated from experimentally found magnetisation curves using formulae (4) and (7) exhibit very good agreement to at least 4 significant digits. The advantage of using DFT is that except for the power losses also the reactive and complex or apparent power can be evaluated that can sometimes be interesting from theoretical point of view (similarly to the complex susceptibility and/or permeability in some relevant cases). Moreover it allows calculation of the total harmonic distortion of driving magnetic field directly from the definition

formula thus allowing to reveal the influence of higher harmonic components to the experimental results.

5. Experimental results

Introductory experiments on Bi-2223/Ag and YBCO based samples have been performed too. The first measurements on the equipment showed promising results and functionality. An example of the measured magnetisation curves is shown in Figs. 5 and 6. YBCO-based sample has been used for the experiment. In Figs. 7 and 8 the measured power losses per unit of strip length with respect to the magnetising flux density magnitude and frequency are shown.

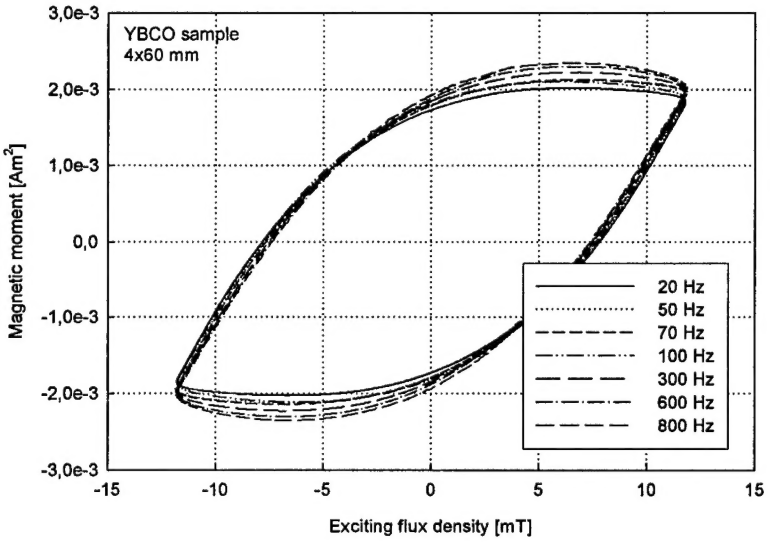

Fig. 5. The example of magnetisation curves at various frequencies, sinusoidal exciting flux density, magnitude 11.82 mT.

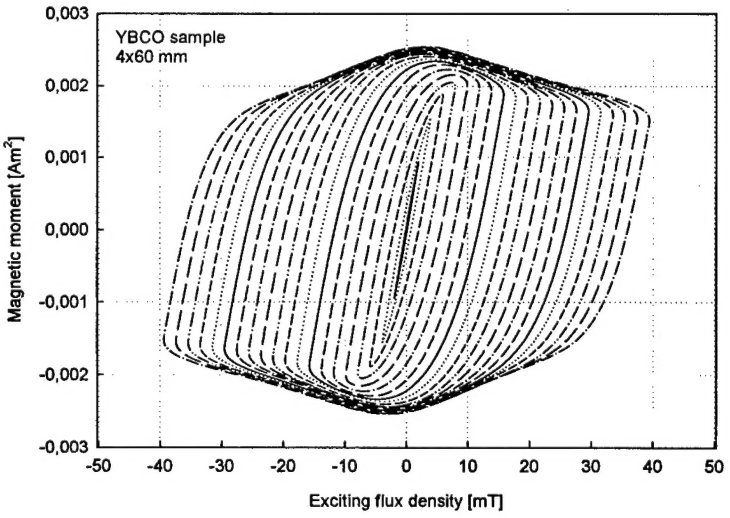

Fig. 6. The example of magnetisation curves at various exciting flux densities (from 1.97 to 39.4 mT, step 1.97 mT), frequency 300 Hz, sinusoidal exciting field.

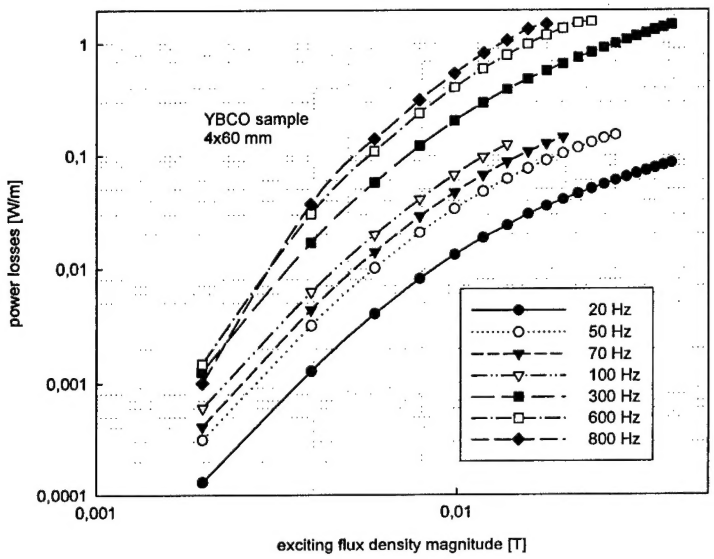

Fig. 7. Power losses versus the magnetising flux density magnitude at various frequencies, sinusoidal exciting field, YBCO sample 4x60 mm.

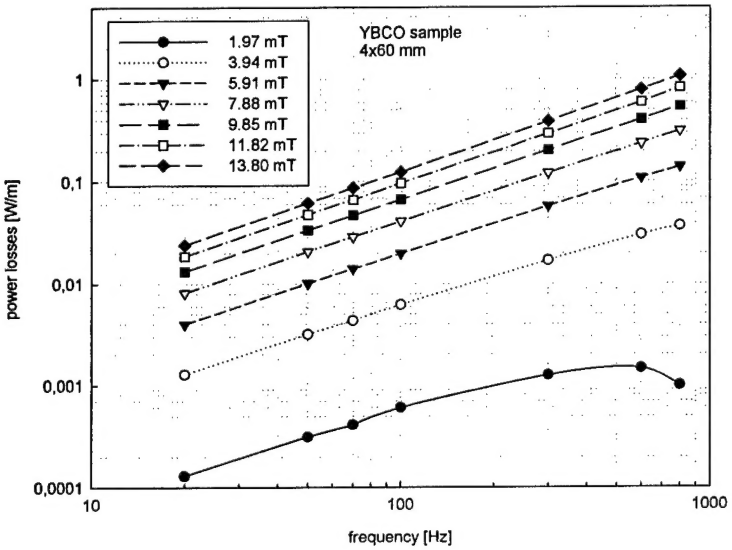

Fig. 8. Power losses versus the frequency at various magnetising flux density magnitudes, sinusoidal exciting field, YBCO sample 4x60 mm.

References:

[1] Ušák, E., Jančárik, V.: Computer-Controlled Hysteresisgraph for Measurement with Arbitrary Signal Waveform, Proceedings of Magnetic Measurements 2000 Conference, Prague, Czech Republic (2000) 33-36
[2] Ušák, E.: Performance Testing of Quasi-Static Digital Hysteresisgraph, Proceedings of the 4th Japan-Central Europe Joint Workshop on Energy and Information in Non-Linear Systems, Brno, Czech Republic (2001) 194-197
[3] Grover, W. F.: Inductance Calculations: Working Formulas and Tables, Dover Publications, Inc., New York, (1946) 60
[4] O'Rourke, J: Computational Geometry in C', Chapter 1, Cambridge Press, (1995).
[5] http://www.brunel.ac.uk/~castjjg/java/polygon/polygon.html.
Ušák, E., Jančárik, V.: Journal of Electrical Engineering **50** (1999) 66-68.

6. Conclusions

Several types of striated samples were prepared and tested.
The transverse resistivity, ρ_{tr}, of samples of striated (filamentary) YBCO tapes prepared within this project very strongly depends on the quality of YBCO/metal layer boundary (stabilizer), characterized by the boundary resistivity, ρ_b, and on the resistivity of this metallic layer.
In samples "as received" the boundary YBCO/metal had quite high resistivity and the shunting effect of the metal was practically negligible. We have found that the heat treatment in O_2 atmosphere improves the boundary properties considerably.
We developed methods to direct as well as indirect determination of the transverse resistivity, based on the measurement of coupling losses.

Declarations

The contractor, Institute of Electrical Engineering, Department of Electrodynamic of Superconductors, hereby declares that, to the best of its knowledge and belief, the technical data delivered herewith under contract F61775-02-W4065, SPC 02-4065
is complete, accurate and complies with all requirements of the contract.

"I certify that there were no subject inventions to declare as defined in FAR 52.227/12, during the performance of this contract."

Date: August 28, 2003
Name and Title of Authorized official: Dr. Milan Polak